Design, Build, and Test of a Simple Motorized CubeSat-Scale Shaker Table

Candace Do, '24

Submitted to the
Department of Mechanical and Aerospace Engineering
Princeton University
in partial fulfillment of the requirements of
Undergraduate Independent Work.

Final Report

May 2, 2023

Michael Galvin
Michael Littman
MAE 340D
82 pages
File Copy

© Copyright by Candace Do, 2023.
All Rights Reserved

This report represents my own work in accordance with University regulations.

Abstract

We are motivated by the problem of developing a simple, cost-efficient shaker table for nanosatellite vibration testing. Satellites must undergo vibration testing to qualify their design for the intense vibration environments of launch. Commercial shaker tables available to rent or buy cost thousands of dollars per test, so we would like to provide a simple, cost-effective solution to universities wishing to bring vibration testing in-house. We propose an electro-mechanical solution consisting of a high-torque, high-speed motor that uses rotational to linear motion to drive a linear stage. We develop a design and prototype of this shaker table solution and provide an assessment of its vibration capabilities. We conclude that this motorized shaker table system is a viable solution for inexpensive in-house vibration testing and provides an accessible testing option for high schools and universities.

Acknowledgements

This endeavour would not have been possible with Michael Galvin, who advised my work this semester and provided invaluable advice and feedback throughout. I am also grateful to to the Department of Mechanical and Aerospace Engineering for funding this project. Many thanks to my friends and family for their support.

Contents

List of Tables

List of Figures

Chapter 1

Introduction

1.1 Background

Vibration tests are a critical component of spaceflight hardware testing. The two main types of vibration testing are random vibration and sine vibration. Random vibration best simulates a real launch environment, while sine testing is useful for identifying flight hardware resonances and providing a worksmanship test. The NASA General Environment Verification Standard (GEVS) [7] describes sine vibration testing as necessary to qualify flight hardware for "low-frequency transient or sustained sine environments" during launch and flight. This project will focus on sine testing since random vibration testing is unattainable with our motorized shaker table system.

In general, NASA GEVS recommends that hardware be qualified to the flight limit vibration level multiplied by 1.25, though specific requirements will vary based on the hardware and launch vehicle. For instance, the SpaceX Falcon 9 rocket has its own vibration profile and recommendations for payload testing as described in the Falcon Users Guide [9].

One common satellite form factor, especially for universities, is the CubeSat. Originally developed by Professors Jordi Puig-Suari at Cal Poly and Bob Twiggs at Stanford, the CubeSat is meant to increase accessibility to space by reducing the cost and time associated with developing satellites. According to the CubeSat Design Specification Rev. 13 (CDS Rev. 13), 1U CubeSats are 10 cm cubes with a mass of up to 1.33 kg [3].

The TigerSats Lab at Princeton is dedicated to developing CubeSats and other nanosatellites, emphasizing methods that promote accessibility to such projects. Tiger-

Sats is looking to bring their nanosatellite test campaigns in-house to reduce time and cost. For instance, Shalaka Madge '21 designed a shock hammer fixture for shock testing of nanosatellites [5]. However, TigerSats still lacks an in-house method of testing nanosatellites under sine vibration.

1.2 Motivation

The TigerSats Lab has previously outsourced vibration testing to Nu Laboratories in Annandale, NJ. The cost to perform three-axis vibration for a single small circuit board was $1425. Princeton's Space Physics Lab also outsourced three-axis vibration testing of a space instrument similar in size to a CubeSat for approximately $9000. These high costs are common for outsourced vibration testing in the commercial space industry. Therefore, there is significant budgetary motivation to create an inexpensive in-house vibration testing method.

1.3 Objectives

The objectives for our shaker table design and prototype are as follows:

1. **The table shall accommodate components up to 10 cm by 10 cm (4 in by 4 in) and up to 1.33 kg.** The CubeSat Design Specification states that 1U CubeSats are 10 cm cubes and weigh up to 2 kg. However, most CubeSats in the TigerSats Lab will be 1 kg or less, so we will relax the mass requirement to 1 kg for testing purposes.

2. **The table shall simulate sinusoidal vibration as described in Table 1.1.** This vibration profile is similar in magnitude to the instrument- and subsystem-level qualification testing ranges specified for NASA flight hardware projects at Princeton University, although the loads are lower to enable an accessible shaker table solution. See Section 2.5 for calculations.

Frequency (Hz)	Acceleration (g)
5	0.60
30	10.88
34	13.97
41	6.77

Table 1.1: Vibration profile requirements.

3. **The system shall minimize cost and be composed of mainly commercial off-the-shelf (COTS) parts, with some custom machined or 3D-printed parts as required, to maximize accessibility to students.** Part of the TigerSats Lab's mission is to democratize nanosatellites for students, and an inexpensive in-house shaker table would provide an accessible means of vibration testing.

Chapter 2

Design Concept

2.1 Design Overview

The shaker table converts the rotational motion of a motor shaft to the linear motion of a linear stage. The motor shaft will be attached to the linear stage via a rod. A CAD model of the system is shown below. CAD models of the linear stage and motor are courtesy of Optics Focus and Applied Motion, respectively.

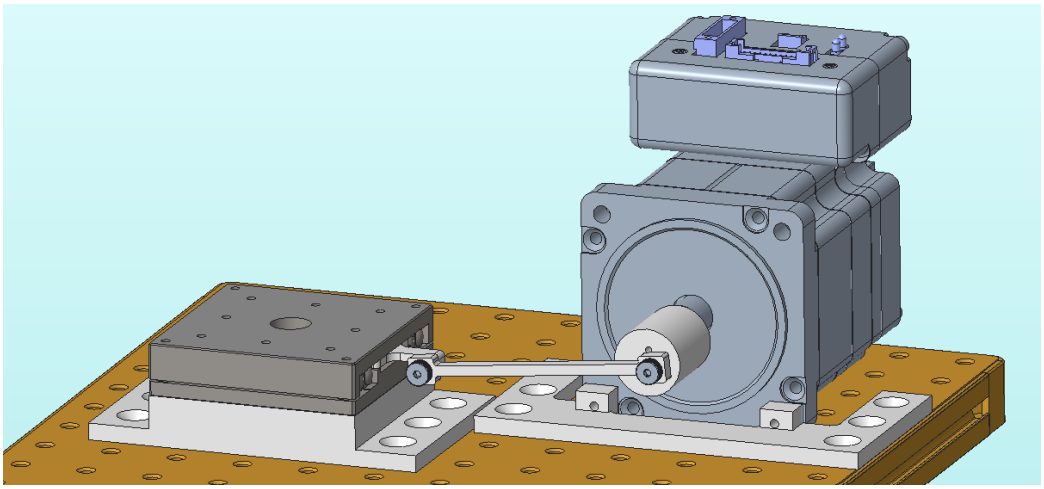

Figure 2.1: Full CAD assembly of shaker table system.

The motor and the linear stage will be commercial-off-the-shelf (COTS) parts. The other components, including the eccentric shaft hub (that attaches to the motor shaft), stage attachment, and connecting crank rod, will be 3D-printed in the prototype and machined in the final version.

2.2 Requirements

The following requirements provide quantitative measures of success.

No.	Requirement	Rationale
1	The system shall be able to create the vibration levels defined in Table 1.1.	While these vibration levels are lower than those during a typical launch in the mid-range (30-40 Hz), this profile is viable for our motorized shaker table solution.
2	The system shall sustain vibration for at least 1 minute.	Typical vibration tests are 1 minute, as described in NASA GEVS Section 2.2.4.
3	The system shall support test articles up to 1.33 kg.	CDS Requirement 3.2.10 defined the max. mass of a CubeSat as 1.33 kg, but many CubeSats weigh less than 1.33 kg and subsystem test articles are less than 1 kg.
4	The system shall support test articles with a base up to 10 cm by 10 cm.	A typical 1U CubeSat has base 10 cm by 10 cm, as defined in CDS Rev. 13 1U CubeSat Acceptance Checklist.
5	The system shall have a manufacturing cost of $1000 or less not including the motor and associated costs.	We would like to provide an inexpensive in-house vibration testing option (see Section 1.2). Users can select a motor to satisfy their vibration profile and budget.
6	The system shall be able to be powered by a typical 120 V wall outlet.	The shaker table should not have special power requirements that cannot be found in a typical high school or university lab.
7	The system shall be be constructed of common materials and should be manufactured without special equipment.	The manufacturing of the shaker table should be easily accessible to the typical high school or university.

Table 2.1: Project requirements.

2.3 Design Process

To begin the design of a shaker table, we first considered several common vibration system designs and conducted a trade study to determine that a motorized system would be the best avenue to pursue (Section 2.4). We then calculated the torque and speeds required of the motor using the vibration environment requirements (Section 2.5). Next, we conducted trade studies to find commercial off-the-shelf components (motor and linear stage) that would satisfy the calculated requirements (Chapter 3). We then designed the remaining components of the shaker table, including the crank rod, stage attachment, eccentric shaft hub, and mounting components for the stage and motor to a breadboard (Chapter 4). We then manufactured and assembled two prototypes (Chapter 5). For our first prototype, used for initial proof-of-concept, these custom components were 3D-printed using PLA. For the second prototype, we replaced the motor and table attachments as well as the crank rod with aluminum. Finally, we tested the system and compared its performance against our expected values, and evaluated the system against the requirements we set in Table 2.1 (Chapter 6).

2.4 System Trade Study

Our first step was to determine the type of system we would design. We considered electrodynamic solutions for designing a shaker table, such as producing vibration via a voice coil. Most commercial shaker tables for large payloads are designed via these solutions. A simpler electrodynamic system could be designed around using a solenoid to actuate a magnetic stage. We also considered electromechanical linear actuator solutions, such as using a motor to drive a linear stage.

When choosing a method, our most important factor was accessibility to students, for whom we would like to democratize nanosatellite testing. This includes lowering cost and time to produce the shaker table as well as difficulty to control the system.

Although voice coils are typically used in industrial shaker tables, they are expensive to procure and can be difficult to control, especially for large test articles.

Solenoids are inexpensive to obtain, but controlling the arbitrary vibration of a payload of an arbitrary mass is a difficult controls problem, especially for high school students who have not taken a controls class. Additionally, making custom solenoids can be very time-consuming.

Finally, a motorized assembly would be easy to control for students. Although

motors can be expensive, the time to assemble would be low since the motor can be bought COTS with usage instructions. Additionally, users can scale the cost and performance of the motor according to their budget and vibration requirements.

The following table summarizes the high-level system trade study.

Method	**Difficulty**	**Cost**	**Time**
Motor	Low	Medium	Low
Solenoid	High	Low	High
Voice coil	Medium	High	Low

Table 2.2: Trade study of shaker table systems.

From this brief trade study, we concluded that a motorized solution would be the most accessible for other students to recreate. In addition, the short timeframe of this project lends to the choice of the motorized solution since it is easy to prototype and iterate.

2.5 Initial Sizing

Several parameters are uniquely determined by the vibration profile. The rotational-to-linear motion mechanism is the same as the reciprocating motion of a piston in an engine, and thus we can use similar equations to model the motion.

Let l be the rod length, r be the crank arm length, x be the position of the linear stage, and θ be the angle between x and r, as shown in Figure 2.2 below.

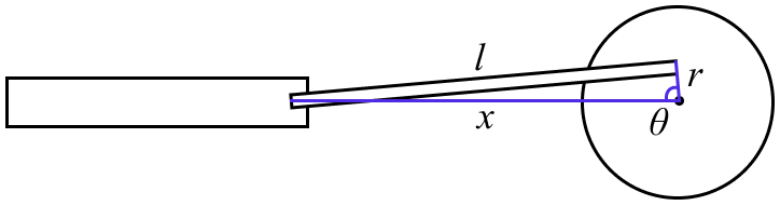

Figure 2.2: Simple diagram of crank rod assembly with linear stage on left, crank rod in center, and eccentric shaft hub (which attaches to motor shaft) on right.

By the law of cosines, we have

$$l^2 = r^2 + x^2 - 2rx\cos\theta.$$

Solving for x yields

$$x = r\cos\theta + \sqrt{l^2 - r^2\sin^2\theta}.$$

Taking the second derivative with respect to the crank angle (which is directly related to time) yields

$$\frac{d^2x}{d\theta^2} = -r\cos\theta + \frac{r^2\cos^2\theta - r^2\sin^2\theta}{\sqrt{l^2 - r^2\sin^2\theta}} - \frac{r^4\sin^2\theta\cos^2\theta}{\left(\sqrt{l^2 - r^2\sin^2\theta}\right)^3}. \tag{2.5.1}$$

As we take the limit $\frac{r}{l} \to 0$ (i.e. $r << l$; the crankarm length is much shorter than the rod length), this approximates as

$$\frac{d^2x}{d\theta^2} = -r\cos\theta$$

which is sinusoidal.

The angle θ is simply the constant rotational velocity ω multiplied by time t: $\theta = \omega t$. Substituting and solving for the acceleration $a = x''$, we obtain

$$|a| = -r\omega^2\cos\theta.$$

The vibration profile only requires the maximum absolute value of the acceleration, which is

$$|a_{\max}| = r\omega^2. \tag{2.5.2}$$

To derive the force required to move the payload at this acceleration, we must multiply by the mass. We assume any hardware required to attach the payload to the linear stage has negligible mass, so multiplying the acceleration by the desired payload capacity m yields

$$|F_{\max}(t)| = m|a_{\max}| = r\omega^2 m. \tag{2.5.3}$$

Because we are given the desired acceleration and the frequency by the vibration levels, this equation uniquely determines the amplitude required for any combination of force and frequency. Table 2.3 shows the required moment arm and motor torque for our vibration levels and a payload mass of 1 kg.

ω **(Hz)**	ω **(rad/s)**	$a_{\max}$ **(g)**	$a_{\max}$**(m/s^2)**	r **(mm)**	$F_{\max}$ **(N)**	τ **(Nm)**
5	31.42	0.63	6.18	6.26	7.11	0.045
30	188.50	22	215.82	5.00	248.19	1.241
34	213.63	22	215.82	4.73	248.19	1.174
41	257.61	1.25	12.26	0.18	14.10	0.003
100	628.32	1.25	12.26	0.03	14.10	0.0004

Table 2.3: Amplitude (A), force ($F_{\max}$), and torque (τ) values given the frequency (ω) and acceleration ($a_{\max}$) based on Equations 2.5.2 and 2.5.3).

However, satisfying some of the amplitude and torque values in the table is not possible with an electro-mechanical, motor-based design. For instance, the vibration level at 41 Hz would require a moment arm of just 0.18 mm, but this approaches machine tolerances of most COTS parts. In addition, motors that can spin at 34 Hz (2040 RPM) and produce a torque of over 1.2 Nm are very expensive. Thus, we will slightly relieve the profile requirements to produce a more achievable design for our physical system. Additionally, according to NASA GEVS Section 2.4.3, most flight hardware is tested up to 50 Hz, so we will not test components up to 100 Hz; we will aim to achieve 41 Hz instead, due to motor limitations. Table 2.4 provides the acceleration levels we can produce with the given amplitudes.

Our system will provide options for amplitudes of 1mm, 3mm, 5mm, and 6mm. Future users can upgrade (or downgrade) their motor appropriately to meet other vibration profiles (loads and frequencies). Users can also machine additional eccentric shaft hubs with more amplitude options.

ω **(Hz)**	ω **(rad/s)**	$a_{\max}$ **(g)**	$a_{\max}$**(m/s^2)**	A **(mm)**	$F_{\max}$ **(N)**	τ **(Nm)**
5	31.42	0.60	5.92	6.0	6.81	0.041
30	188.50	10.88	106.59	3.0	122.58	0.368
34	213.63	13.97	136.91	3.0	157.45	0.472
41	257.61	6.77	66.36	1.0	76.32	0.076

Table 2.4: Acceleration ($a_{\max}$), force ($F_{\max}$), and torque (τ) values given the frequency (ω) and amplitude (A) based on Equations 2.5.2 and 2.5.3).

Comparing the values in Tables 2.3 and 2.4, we can see that we have a reasonably accurate acceleration at 5 Hz. The acceleration values at 30 and 34 Hz are approx-

imately half of what is desired, and the acceleration at 41 Hz is approximately five times of what is desired. Note that 6.77 g is a conservative over-test for hardware that is only required to survive 1.25 g at 41 Hz.

Chapter 3

COTS Component Selection

3.1 Motor Selection

To select a motor, we first determined the best type of motor for this application. Common electric motors include brushed DC motors, brushless DC motors, stepper motors, and servos. Our system requires a motor with precise speed control (to precisely reach the desired frequencies), high speed (to reach high frequencies), and high torque (to drive a heavy payload at high accelerations).

Stepper motors provide precise positional control by rotating the motor shaft in a precise number of steps. Generally, stepper motors can provide high torque at low speeds, but torque falls off at high speeds. They are commonly used in robotics and automation applications.

Servo motors provide precise position, speed, and torque control using internal feedback mechanisms. They also provide high torque at low speeds. They are commonly used in robotics and industrial applications.

Brushed DC motors use brushes and commutators to rotate the motor shaft. They are more simple and less expensive than the other types of motors mentioned, and are often used in common household applications. Brushed DC motors typically do not offer precise control without a separate speed sensor.

Finally, brushless DC motors have permanent magnets on the rotor and electromagnets on the stator. Three coils, controlled by the motor driver, inside the motor generate a magnetic field that makes the motor shaft turn. Hall sensors detect when the current should switch, controlling the speed of the motor. Brushless DC motors are more complex than brushed DC motors but can provide high torque at high

speeds. They are often used in industrial applications.

The following table summarizes the characteristics of each type of motor and its suitability for our applications in five categories: integral speed control, high torque, high speed, cost, and lifespan.

Type	Speed Control	High Torque	High Speed	Cost	Lifespan
Brushless DC	Yes	Yes	Yes	High	Long
Stepper	Yes	Yes	Some[1]	High	Long
Servo	Yes	Some[2]	Yes	High	Long
Brushed DC	No	Some[3]	Yes	Low	Short

Table 3.1: Motor type trade study.

Based on this brief trade study, a brushless DC motor is the best choice for this project. Brushless DC motors have precise speed control though built-in speed sensors (usually through integral Hall sensors), as well as the high torque and speed required for intense vibration. They also have long lifespans. One downside to using brushless DC motors is the cost; the motor and associated components (driver and power supply) would likely be the largest costs associated with the project. Brushless DC motors are also more complex and difficult to control than the other motor types.

Our initial motor choice was the BL34E34-01D-05RO brushless DC motor manufactured by Lin Engineering, which includes a built-in encoder for precise speed control in addition to its Hall sensors. This motor has the added benefit of a compatible motor controller/driver, Lin Engineering's BLDC100. This motor controller provides analog or digital control of the motor speed. A summary of this motor's relevant specifications are shown in Table 3.2.

We bought both the BL34E34 motor and the BLDC100 motor controller from DigiKey. Upon receiving the motor and controller, however, we were unable to operate the motor after following the instructions from Lin Engineering. After two weeks of attempting to get this motor system working, with assistance from Jon Prevost and technicians from Lin Engineering, we decided that our efforts were better spent on an alternative motor. All parties suspected that the Hall sensors were incorrectly wired

[1]Most stepper motors are designed for low-speed operation.
[2]Some servo motors have limited torque at high speeds.
[3]Torque depends on current draw. Brushed DC motors generally have lower torque output than brushless DC motors.

by the manufacturer, but we did not want to invalidate the warranty and return eligibility of the motor by taking it apart to investigate.

Rated speed	66.67 rps
Maximum speed	75 rps
Rated torque	0.72 Nm
Max torque	1.44 Nm
Rated current	7.49 A
Rated voltage	48 VDC
Communication	RS-232

Table 3.2: Specifications for the Lin Engineering BL34E34-01D-05RO motor. Courtesy of Lin Engineering [6]. Imperial units have been converted to metric units.

Fortunately, the TigerSats Lab had a large stepper motor that had similar torque and speed capabilities as the brushless DC motor. As seen in Table 3.1, a stepper motor also satisfies the requirements of speed control, high torque, and high speed. The drawback of a stepper motor is that its speed control is accomplished via precise positional control of the number of steps. This precise positional control is superfluous since we only require precise speed control. In addition, most stepper motors are designed for low-speed operation, which makes high-speed stepper motors expensive.

However, we decided to use this motor for the time being so that we could produce a prototype of the system before the semester ended. This stepper motor, the TSM34Q-1AG from Applied Motion (as shown in Figure 3.1), boasts high torque capabilities, and can operate at speeds up to 50 rps. The motor's torque curve is provided in Figure 3.2. Below is a summary of this motor's specifications.

Maximum torque	3.00 Nm
Rated current	3 A
Supply voltage	24-70 VDC
Encoder resolution	5000 lines (20,000 counts quadrature)
Step angle	1.8 degrees
Communication	RS-232

Table 3.3: Specifications for the Applied Motion TSM34Q-1AG StepSERVO motor. Courtesy of Applied Motion [2].

This motor package also includes the motor driver, which can be programmed using Q programming in Applied Motion's software through RS-232 communication.

Figure 3.1: Applied Motion TSM34Q-1AG StepSERVO motor. Courtesy of Applied Motion [2].

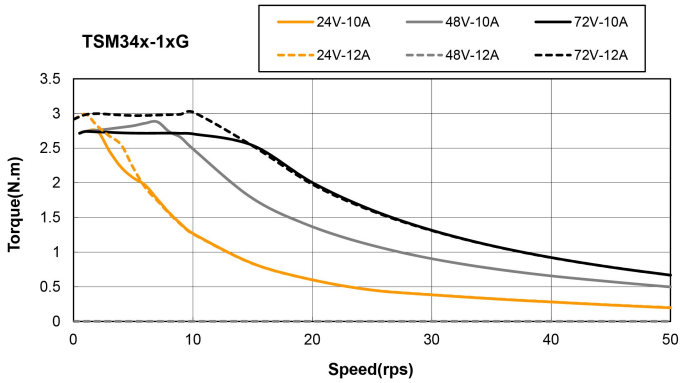

Figure 3.2: Applied Motion TSM34Q-1AG StepSERVO torque curve. Courtesy of Applied Motion [2].

We began by using the PS150A-24 power supply from Applied Motion, but later switched to the PS480D72 power supply so that our motor could draw higher current and thus produce more torque. Both power supplies can use input power from a typical 120V wall outlet.

3.2 Linear Stage Selection

The second COTS component of the shaker table system is a linear stage, which vibrates horizontally and supports the payload. Since the linear stage must operate freely with low friction, we chose to modify a COTS one-axis manual optical positioning stage, which are typically used for high-precision optical applications but possess the characteristics we require for this project.

Typical linear translation stages use crossed-roller bearings or ball-bearings to achieve low-friction, tight-tolerance movement, and manual stages are driven by precision micrometers. For our shaker table prototype, we chose to use the MAX-80C-25 manual positioning stage from Optics Focus, shown in Figure 3.3. The main characteristics that differentiated this particular linear stage from other potential options (e.g. from ThorLabs) was the relatively low price and the size of the table, which at 8 cm by 8 cm is close to the size of a 1U CubeSat.

Figure 3.3: MAX-80C-25 manual positioning stage from Optics Focus. Courtesy of Optics Focus [8].

To modify the linear stage for our needs, we removed the micrometer and internal springs, as well as any extraneous screws or knobs. A breakdown of the linear stage is shown in Figure 3.4.

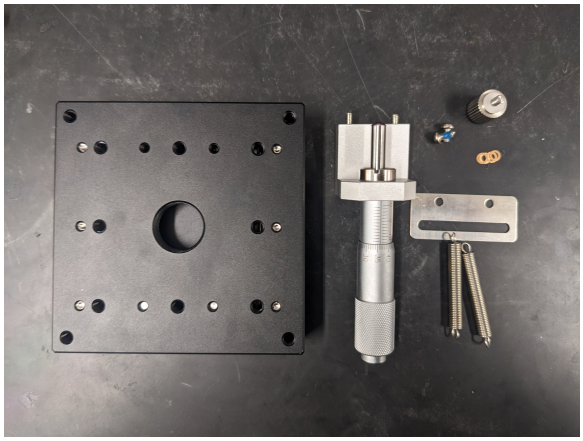

Figure 3.4: Components of linear stage. From left to right: main stage, micrometer, extraneous springs and other components.

The modified linear stage provides a smooth one-axis linear motion with a stage large enough to accommodate a 10 cm by 10 cm CubeSat.

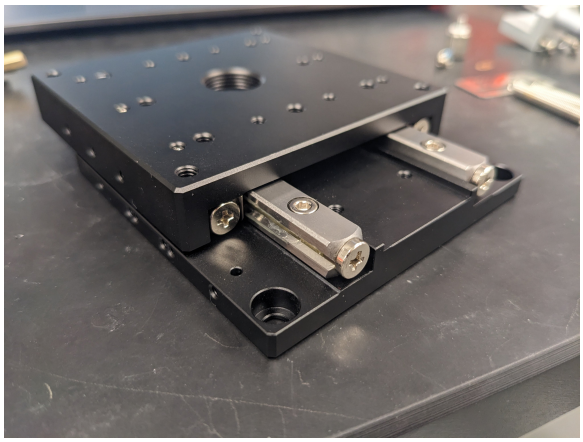

Figure 3.5: Modified linear stage with crossed-roller bearings exposed.

Chapter 4

Custom Component Design

A few custom-designed components connect the motor and linear stage. These include the crank rod, eccentric shaft hub, attachment from the rod to the linear stage, and the motor and stage mounts. For each of the components, we designed one version for the 3D-printed prototype, and we also designed a second version for the machined prototype.

The CAD of the full system with machined parts is shown in Figure 2.1.

Drawings for all custom-designed machined components are provided in Appendix A.

4.1 Use of Shoulder Screws

Our design uses shoulder screws as shafts for connection between the eccentric shaft hub and the crank rod as well as between the crank rod and the stage attachment. We designed this for our initial prototype with the awareness that screw back-out could be an issue given the vibration of the system; however, shoulder screws provided a relatively inexpensive and easy-to-assemble prototype. When we tested the machined prototype, we found that with sufficient tightening torque, screw back-out was not an issue, so we decided not to replace the high-friction plain bearings with low-friction ball bearings in our machined prototype.

We did also design a ball bearing-based alternative to the shoulder screws in case the screw back-out proved to be an issue. This design is discussed further in Section 7.2.4. When testing the shoulder screw prototype, we found that friction was wearing down the shoulder screw and crank rod to produce some metal dust. This

did not cause any issues during testing, but may be an issue for long-term use, so implementing the ball bearing design would make the system more robust.

4.2 Eccentric Shaft Hub

The eccentric shaft hub not only connects the crank rod to the motor, but also allows the user to change the amplitude (and thus load level) of the vibration. For the initial prototype, we chose to create amplitudes of 1 mm, 3 mm, 5 mm, and 6 mm. The amplitudes of 1 mm, 3 mm, and 6 mm were those used in Table 2.4 to create the required load levels. The additional 5 mm amplitude can be used to create additional load levels.

Figure 4.1 below shows two views of the CAD of the 3D-printed eccentric shaft hub. View 1 shows the four possible attachment points for the crank rod on the front face. They are spaced at distances from the center of the face such that the vibration amplitudes will be 1 mm, 3 mm, 5 mm, and 6 mm as described earlier. In the 3D-printed version, threaded heat-set inserts were placed inside these holes. View 1 also shows a hole for the motor shaft set screw on the side of the cylinder. Another heat-set insert was placed to secure the set screw. Finally, View 2 shows the hole for the motor shaft on the back face of the motor.

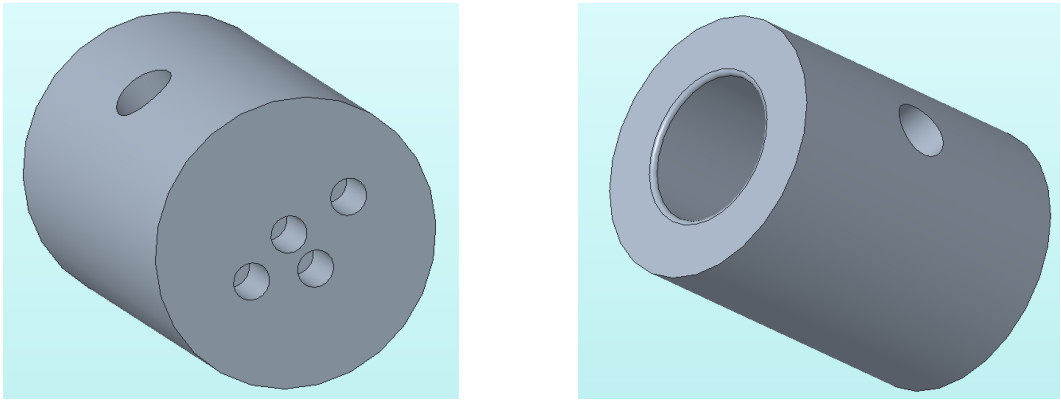

(a) View 1 **(b)** View 2

Figure 4.1: CAD of 3D-printed eccentric shaft hub.

For the machined version, we resized and threaded the holes for the appropriate screws. We also removed the rounding on the motor shaft hole since this is not easily machinable. In addition, we changed the shoulder screws from M2 screws with 3 mm diameters to M3 screws with 5 mm diameters. When testing the 3D-printed prototype, we found that the shoulder screw would sometimes "back out" of

the threaded hole due to the intense vibration. Thus, for the machined version, we wanted to maximize the bearing surface area between the face of the shoulder screw and the face of the eccentric shaft hub to prevent the screw from backing out. This was achieved with higher preload and locking friction torque.

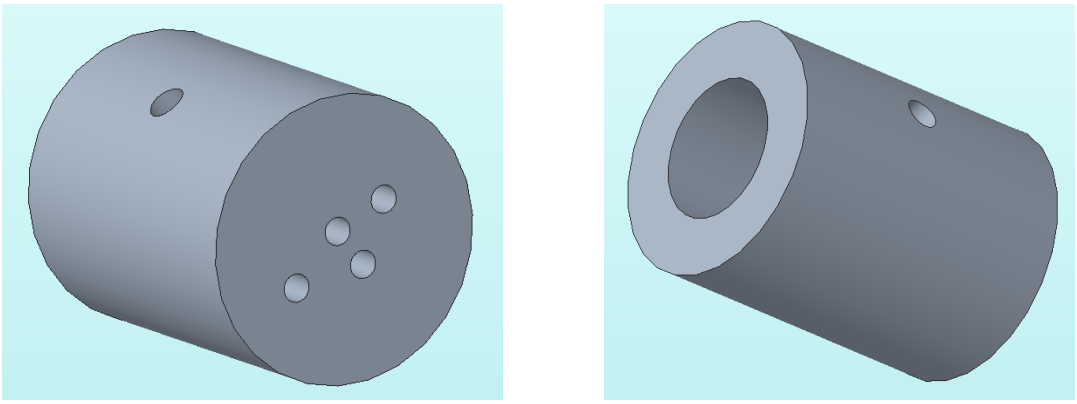

(a) View 1 **(b)** View 2

Figure 4.2: CAD of machined eccentric shaft hub.

4.3 Linear Stage Attachment

The linear stage attachment serves to connect the crank rod to the linear stage. It is custom-designed to attach to the MAX-80C-25 linear stage's mounting holes.

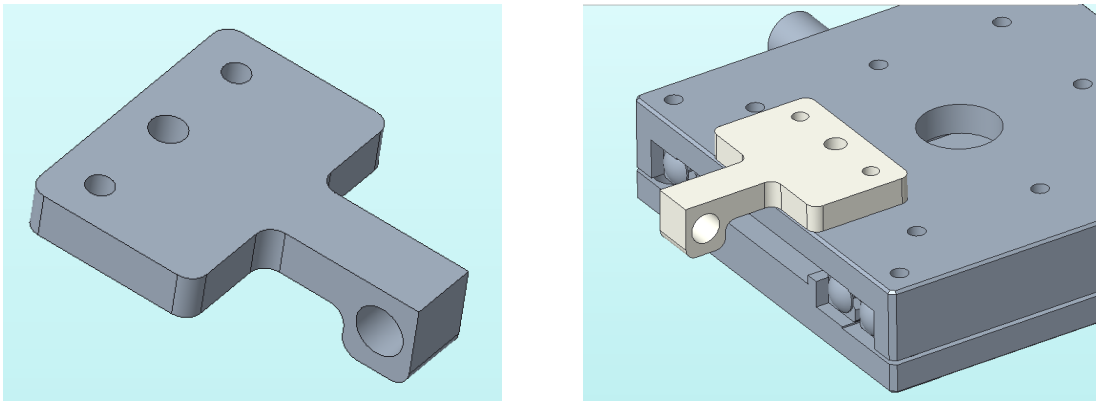

(a) Close-up of stage attachment. **(b)** Attachment in assembly with stage.

Figure 4.3: CAD of 3D-printed stage attachment.

In the machined version of the linear stage attachment, we decided to move the attachment to the bottom face of the stage to maximize the space available on top

for the payload. To make the stage attachment fit, we had to swap our regular screws for flathead screws and drill countersinks into the piece, as seen in Figure 4.4 below.

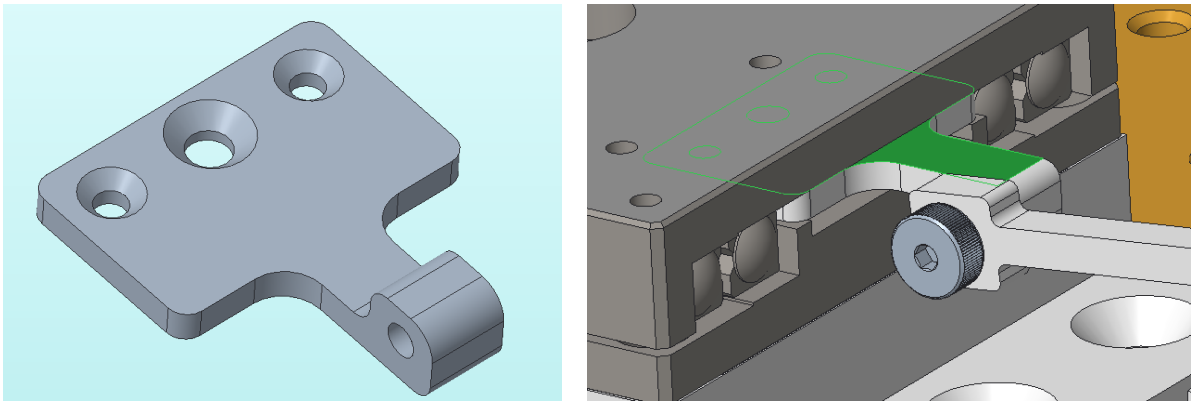

(a) Close-up of stage attachment. **(b)** Attachment in assembly with stage.

Figure 4.4: CAD of machined stage attachment.

4.4 Crank Rod

The crank rod connects the motor and the linear stage. Shoulder screws fit into the two holes at the ends of the crank shaft and screw into the eccentric shaft hub at one end and the stage attachment at the other end (see Figure 4.7).

In the 3D-printed version (shown in Figure 4.5), the shoulder screw connecting to the eccentric shaft hub is slightly smaller than the the shoulder screw connecting to the stage attachment (3 mm diameter vs. 5 mm diameter).

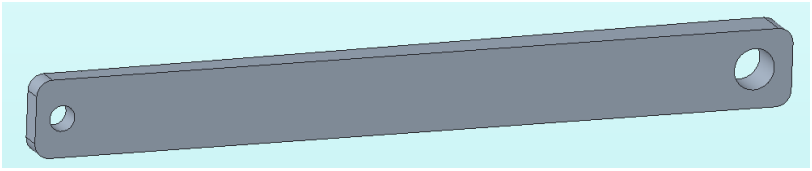

Figure 4.5: CAD of 3D-printed crank rod.

In the machined version (shown in Figure 4.6), both shaft holes fit a 5 mm shoulder screw. This change both increased the contact area between the shoulder screw and motor/stage attachments as well as standardized the hole size for this part.

We were particularly concerned about friction torque between the shaft hole on the crank rod and the shoulder screws. To err on the side of caution when outsourcing the machining of this part, we opted for a free fit on this shaft, so the diameter of the shaft hole is 5.25 mm.

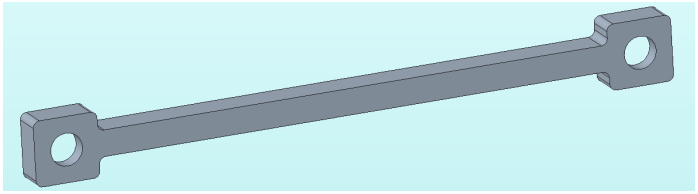

Figure 4.6: CAD of machined crank rod.

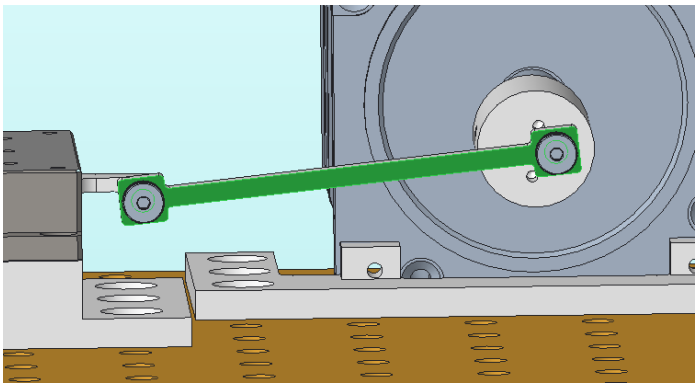

Figure 4.7: Crank rod in assembly.

Compared to the eccentric shaft hub and the stage attachment, the crank rod is the most likely to fail under stress. We performed a quick stress analysis on the crank rod using Creo Simulate with a static load. Though the load on the crank rod will primarily be fast transient periodic loads, we approximate these with a static load and add a safety factor of 2.

To perform the analysis, we constrained the left end of the crank rod and applied a load on the right end. Note that the tensile yield strength of Aluminum 6061 is 276 MPa [1]. Under the maximum predicted load of approximately 150 N from Table 2.4, the maximum stress was about 14 MPa, as shown below.

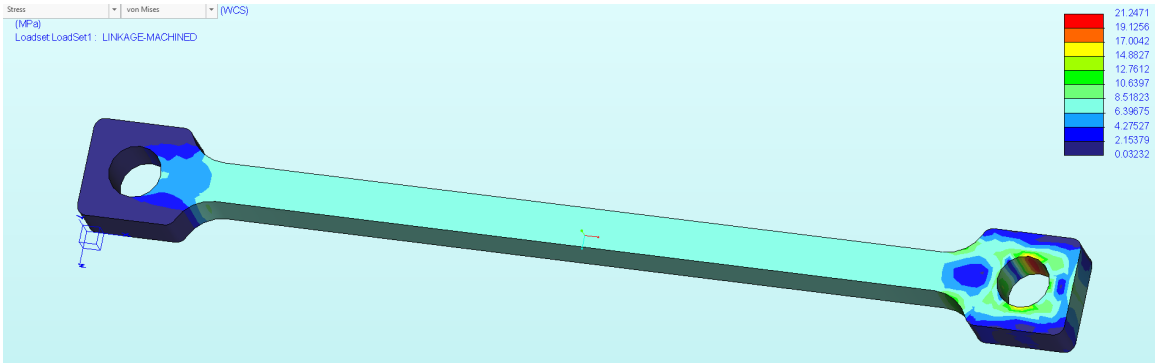

Figure 4.8: Crank rod under 150 N load.

Assuming a safety factor of 2, we can bring the stress in the crank rod up to 138 MPa. Under a load of 1200 N, the maximum stress is about 130 MPa.

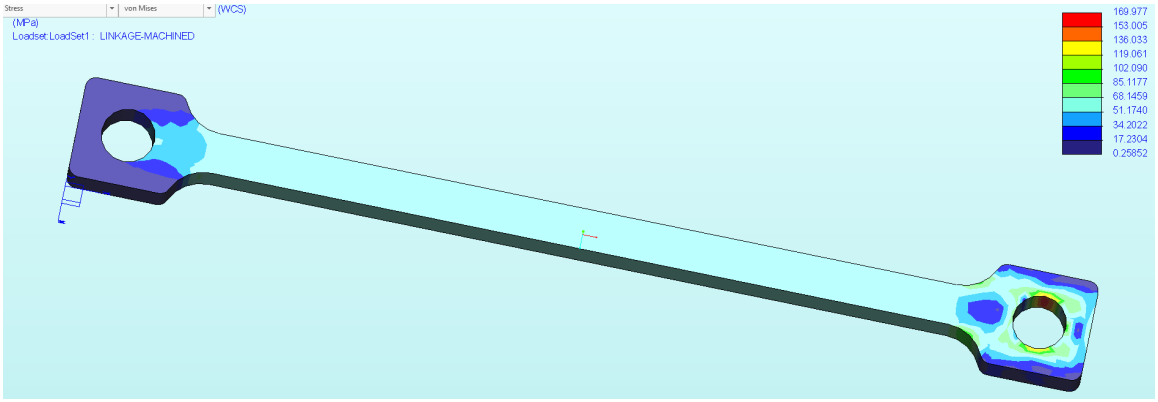

Figure 4.9: Crank rod under 1200 N load.

We also calculated a simple buckling analysis of the crank rod, keeping in mind that bucking analyses are primarily for static loads. Euler's buckling formula states that the buckling force is

$$F = \frac{n\pi^2 EI}{L^2}$$

where n is the buckling mode, E is the modulus of elasticity, L is the length of the beam, and I is the moment of inertia. We assume that the crank rod is pinned at both ends, so $n = 1$. The modulus of elasticity of Aluminium 6061 is 68.9 GPa, the length of the rod is 100 mm = 0.1 m, and the moment of inertia is $I = \frac{1}{12}(0.004)^3 \cdot (0.005) = 2 \times 10^{-11}$ m^4. Thus, we have

$$F_{\text{buckling}} = \frac{\pi^2(68.9 \times 10^9)(2.67 \times 10^{-11})}{0.1^2} = 1816 \text{ N}.$$

Under a safety factor of 2, even a load of 22 g at 34 Hz would not achieve this buckling load. Thus, we predict that this crank rod will suffice for our vibration tests. If future users would like to put higher loads on the system, they can thicken the neck of the crank rod to reduce stress.

Finally, we calculated the fundamental frequency of the crank rod to ensure it does not conflict with the frequency range we plan to test. The equation for the fundamental frequency of a pinned-pinned beam is

$$f = \frac{1}{2\pi}\left(\frac{\pi}{L}\right)^2 \sqrt{\frac{EI}{\rho_L}}$$

where ρ_L is the linear mass density [4]. We have $\rho_L = (0.004 \text{ m})(0.005 \text{ m})(2700 \text{ kg/m}^3) = 0.054 \text{ kg/m}$. The fundamental frequency is

$$f = \frac{1}{2\pi}\left(\frac{\pi}{0.1}\right)^2 \sqrt{\frac{(68.9 \times 10^9)(2.67 \times 10^{-11})}{0.054}} = 917 \text{ Hz}.$$

This is a much higher frequency than the frequency range we plan to test (or most reasonable frequency ranges for sine vibration testing).

4.5 Motor and Stage Mounts

Finally, the motor and stage mounts fasten the motor and linear stage down to a 1/4"-20 breadboard. The current prototype uses 3D-printed versions of the mounts, shown in Figure 4.10. We have also designed machinable versions of the mounts to be manufactured for a future version of this system, but did not have enough time or budget to obtain the actual machined parts.

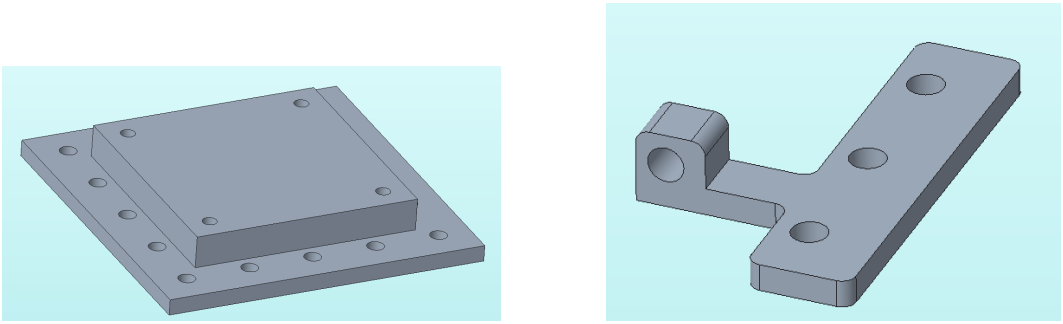

(a) 3D-printed version of stage mount. **(b)** Right portion of 3D-printed motor mount.

Figure 4.10: CAD of 3D-printed stage mount and motor mount.

When designing the machined versions of the stage and motor mounts, we tried to reduced the cost of machining. For the stage mount, we reduced the size of the piece by removing mounting holes on two sides of the mount, as shown in Figure 4.11a. For the motor mount, we connected the two halves of the 3D-printed mount to create a single piece as shown in Figure 4.11b, which is typically cheaper to machine than two separate pieces.

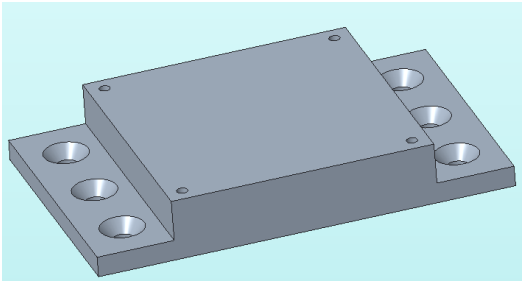

(a) Machinable stage mount.

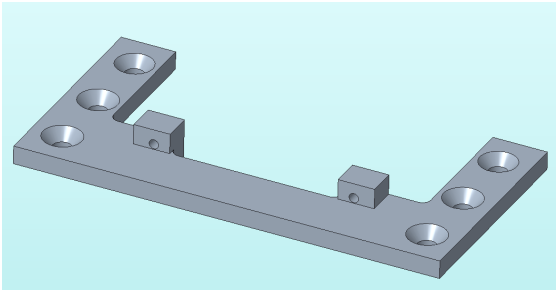

(b) Machinable motor mount.

Figure 4.11: CAD of machinable stage mount and motor mount.

Chapter 5

Manufacturing and Assembly

5.1 3D-printed Prototype

For the initial prototype, all custom components were 3D-printed on an Ender 3 Pro printer using PLA filament. All components were printed with 70% gyroid infill for additional strength. The 3D-printed eccentric shaft hub, stage attachment, and crank rod are shown in Figure 5.1 below, with heat-set inserts installed.

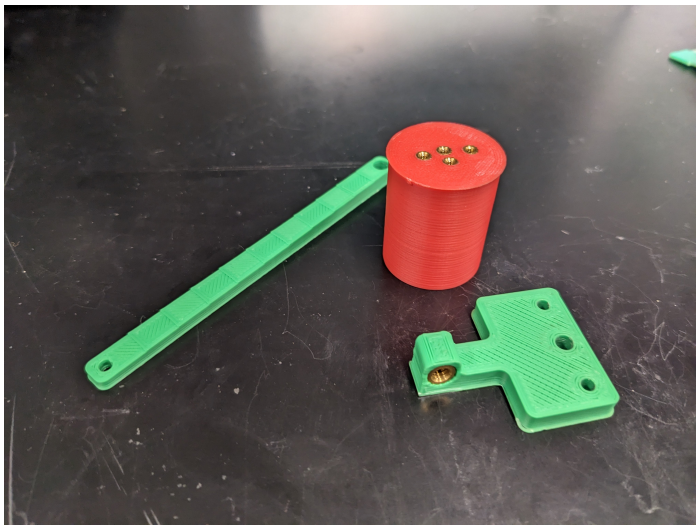

Figure 5.1: 3D-printed components. From left to right: crank rod, eccentric shaft hub, and stage attachment.

Most of the components printed with no issues. The largest component, the stage mount, had some warping issues, and the mounting holes did not match the breadboard's hole pattern exactly. However, we were still able to fasten the mount

to the breadboard after drilling out some of the 3D-printed holes. Figure 5.2 shows the misalignment of some of the stage mount holes. The misalignment is particularly clear in the center 3 holes shown in the image.

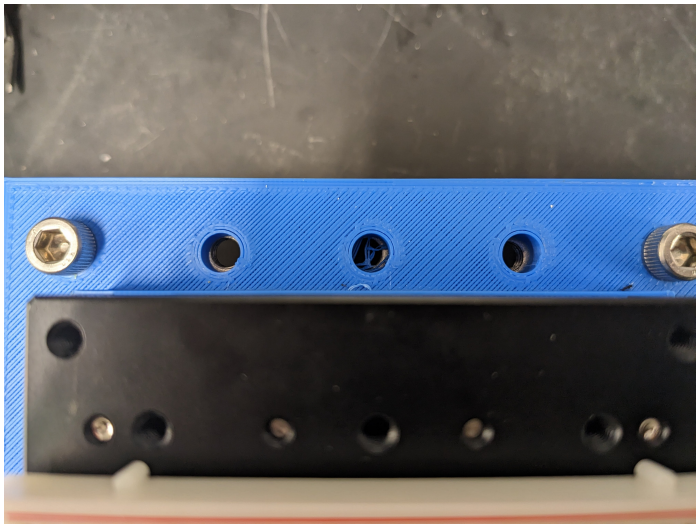

Figure 5.2: Misalignment of 3D-printed stage attachment holes.

The 3D-printed assembly (without the motor mount, which had not been printed at the time of this photo) is shown in Figure 5.3.

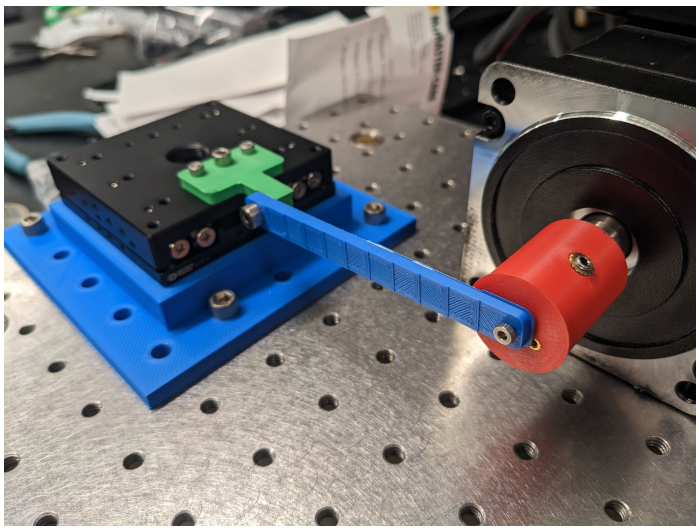

Figure 5.3: 3D-printed prototype.

5.2 Machined Prototype

Our three machined parts (eccentric shaft hub, stage attachment, and crank rod) for our second prototype were machined by Xometry. We quoted these three parts with both Xometry and Protolabs, and Xometry was able to produce the parts for a lower cost and faster speed.

The machined assembly is shown in Figure 5.4 below. As mentioned in Section 4.5, we did not have time to machine the motor and stage mounts, so they remained 3D-printed for this prototype.

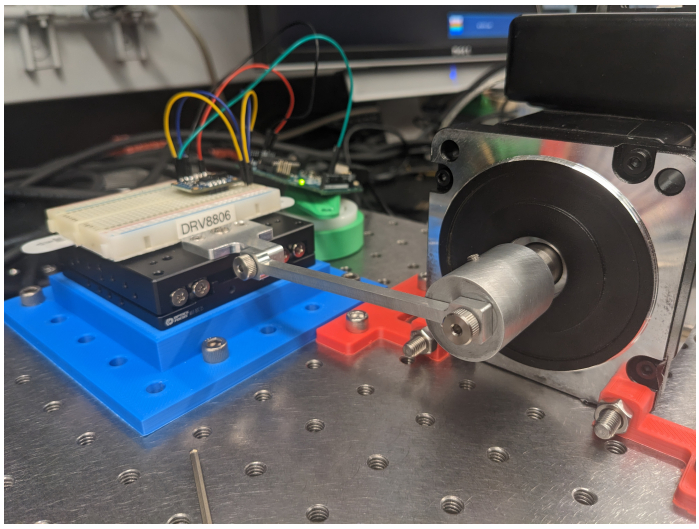

Figure 5.4: Machined prototype.

As mentioned in Section 4.4, we machined the crank rod shaft holes to have a free fit around the 5 mm shoulder screws. When we assembled the crank rod with the shoulder screws in the full system, we found that there was noticeable space between the shaft hole and the shoulder screw; we were able to jiggle the crank rod around the shoulder screws. Overall, this was not a major issue, but did cause some discrepancies with the expected acceleration values as described in Section 6.4.

Chapter 6

Testing, Results, and Discussion

6.1 Accelerometer Setup

To verify our prototype's performance against our requirements, we measured the acceleration experienced by a payload on our shaker table system using an accelerometer. We chose to use the Invensense MPU-9250, which includes a 3-axis accelerometer, a 3-axis gyroscope, and a 3-axis compass. We chose to use the MPU-9250 over other IMUs available in the TigerSats Lab (such as the Adafruit BNO055) because it has a high read-out rate (up to 4k Hz) and can sense accelerations up to 16 g.

We placed the IMU on a small breadboard and taped it securely onto the linear stage, as shown in Figure 6.1.

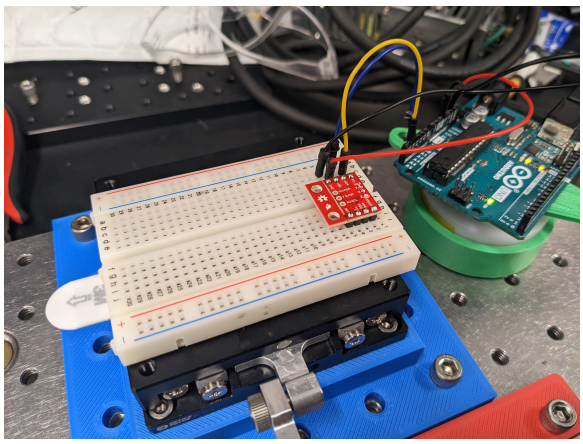

Figure 6.1: MPU-9250 IMU secured onto linear stage.

We read out data from the accelerometer using an Arduino Uno. The Arduino code used is shown in Appendix B.

6.2 Data Collection Methods

We collected two sets of data: one set for no payload (besides the IMU and breadboard, which have negligible mass) and a second set for a 1 kg payload, which we simulated with a 1 kg brass block, machined by Xometry, shown in Figure 6.2. As mentioned in Table 2.1, this is a reasonable proxy for a CubeSat that complies with the CDS Rev. 13 maximum mass requirement of 1.33 kg.

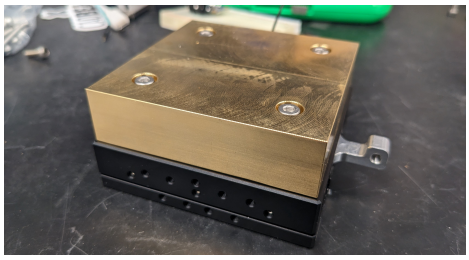

Figure 6.2: 1 kg brass block to simulate payload mass, shown attached to the linear stage.

We collected data for the frequencies and crank arm lengths described in Table 6.1. These particular combinations of frequencies and crank arm lengths were chosen to test a full range of frequencies and loads as well as to verify the vibration profile requirements in Table 1.1. We also conducted several tests for 1 minute to ensure that the system could sustain one minute of vibration.

Frequency (Hz)	**Crank Arm Lengths (mm)**
5	3, 5, **6**
10	1, 3, 5, 6
15	1, 3, 5, 6
20	1, 3, 5
25	3
30	**3**
34	**3**
35	3
40	1
41	**1**

Table 6.1: Frequencies and crank arm lengths tested. Bolded entries are those that were predicted to satisfy the vibration profile.

6.3 Results

6.3.1 No Payload

The graphs in Figures 6.3 to 6.6 show the acceleration of the shaker table over time for the frequencies and crank arm lengths chosen to produce the vibration profile requirement (bolded in Table 6.1). In the subfigures on the left, the blue line shows the measured acceleration, and the orange line shows the expected acceleration from our calculations in Section 2.5. We chose a small time range for these subfigures (10 cycles each) to better visualize the comparison between measured and expected values. The subfigures on the right show a larger time range of the measured acceleration values to demonstrate the consistency of the vibration. The code used to produce the following graphs is shown in Appendix B.2. Additional graphs for the other vibration tests are shown in Appendix D.

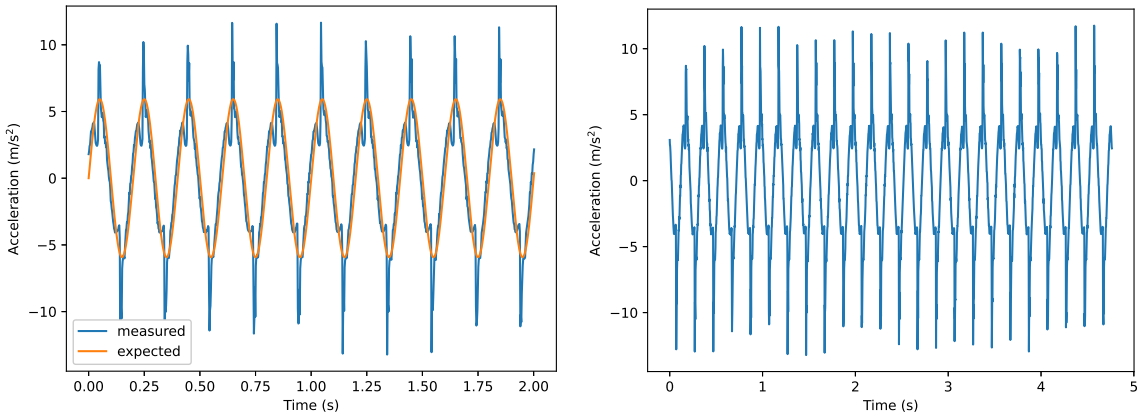

(a) Measured vs. expected comparison.

(b) Measured acceleration.

Figure 6.3: Acceleration data for frequency 5 Hz, crank arm 6 mm, no payload. The orange line describes the expected acceleration, while the blue line describes the measured acceleration.

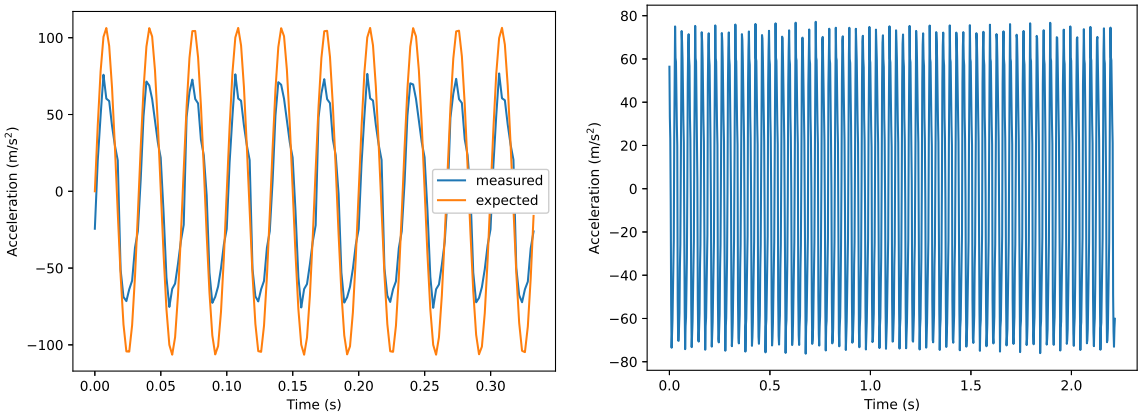

(a) Measured vs. expected comparison. **(b)** Measured acceleration.

Figure 6.4: Acceleration data for frequency 30 Hz, crank arm 3 mm, no payload.

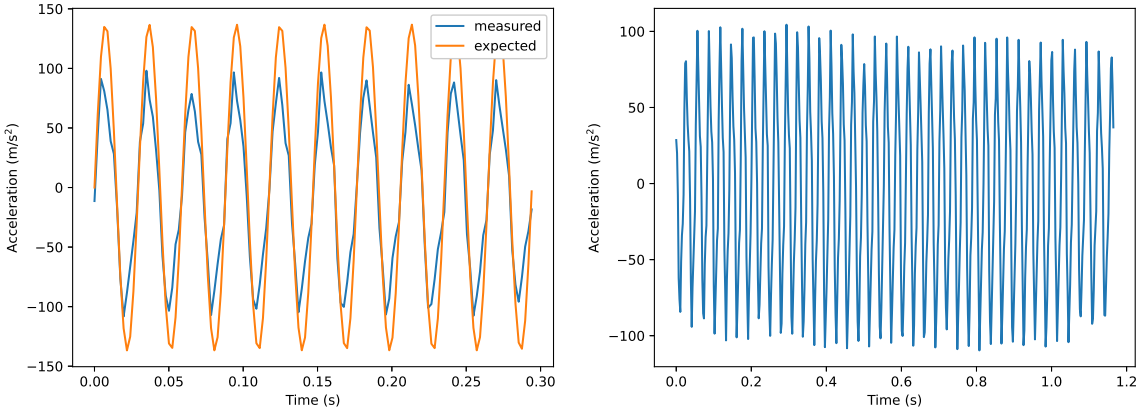

(a) Measured vs. expected comparison. **(b)** Measured acceleration.

Figure 6.5: Acceleration data for frequency 34 Hz, crank arm 3 mm, no payload.

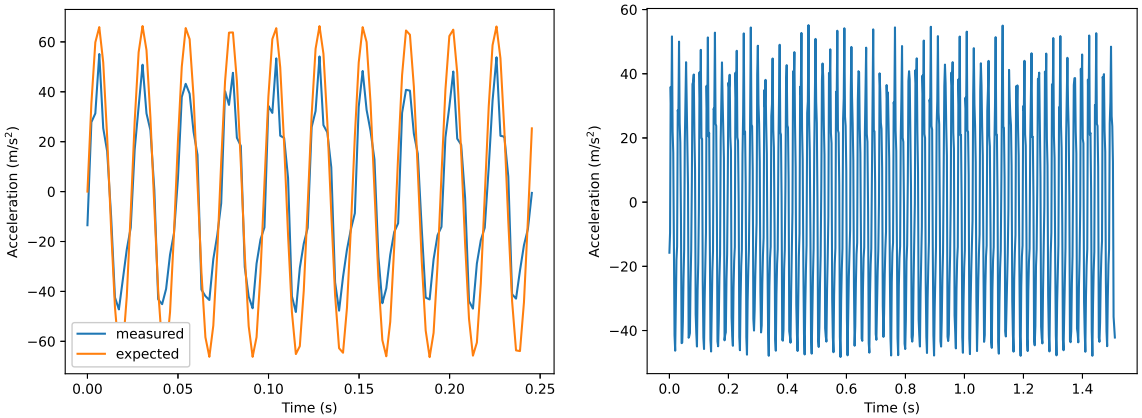

(a) Measured vs. expected comparison. **(b)** Measured acceleration.

Figure 6.6: Acceleration data for frequency 41 Hz, crank arm 1 mm, no payload.

We compared the average measured peak acceleration of the vibration against the expected acceleration as described in Section 2.5. We found the peak accelerations for 10 cycles of each test using `scipy`'s `signal.find_peaks()` function. Then, we calculated the average peak for the 10 peaks and the standard deviation. Finally, we found the percentage error of the measured peak versus the expected peak:

$$\text{Percentage error} = \frac{\text{Measured avg. peak accel.} - \text{Expected peak accel.}}{\text{Expected peak acceleration}} \times 100\%.$$

This data is provided in Table 6.2. The code is provided in Appendix B.2.

Freq. (Hz)	Arm (mm)	Expected Peak (m/s^2)	Meas. Avg. Peak (m/s^2)	St. Dev. (m/s^2)	% Error
5	3	2.96	6.82	0.56	+130.2
	5	4.94	8.07	0.43	+63.5
	6	5.92	10.90	0.67	+84.1
10	1	3.95	7.81	0.41	+97.9
	3	11.34	18.20	0.91	+60.5
	5	19.74	23.92	0.87	+21.2
	6	23.68	27.78	0.48	+17.3
15	1	8.88	14.63	1.28	+64.8
	3	26.64	31.54	1.22	+18.4
	5	44.41	41.49	0.73	−6.6
	6	53.29	49.23	0.51	−7.6
20	1	15.79	21.76	0.55	+37.8
	3	47.03	43.27	1.90	−8.0
	5	78.96	63.14	0.16	−20.0
25	3	74.02	59.73	2.33	−19.3
30	3	106.46	73.40	1.97	−31.1
34	3	136.74	90.78	5.49	−33.6
35	3	145.06	83.75	2.64	−42.3
40	1	63.16	48.07	2.43	−23.9
41	1	66.36	49.56	4.60	−25.3

Table 6.2: Average measured peaks for each no-payload vibration test compared to the expected peaks.

6.3.2 1 kg Payload

The graphs in Figures 6.7 to 6.10 show the acceleration of the shaker table for the vibration tests with the 1 kg payload (brass block) attached to the linear stage. Additional acceleration data is shown in Appendix D.

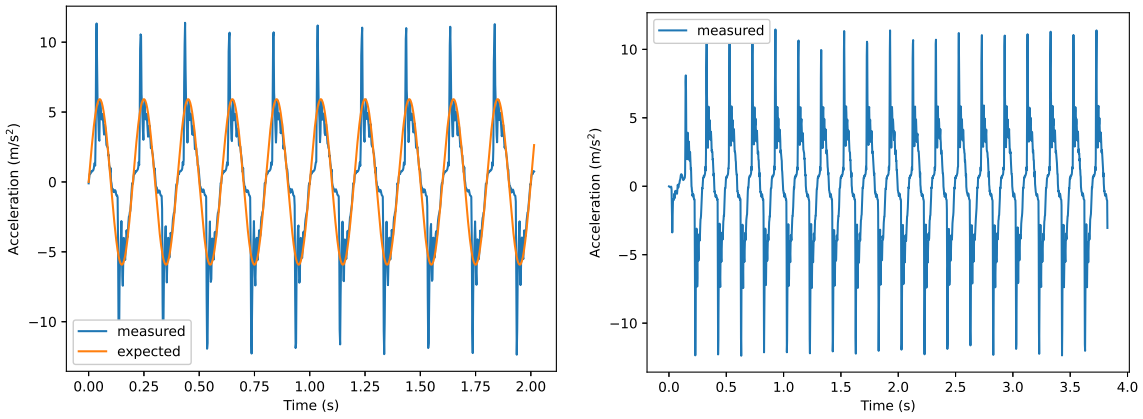

(a) Measured vs. expected comparison. **(b)** Measured acceleration.

Figure 6.7: Acceleration data for frequency 5 Hz, crank arm 6 mm, 1 kg payload.

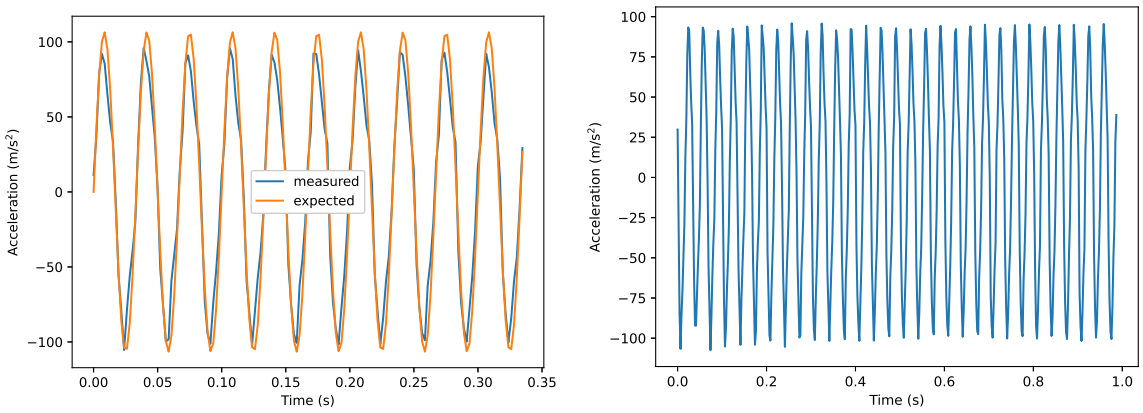

(a) Measured vs. expected comparison. **(b)** Measured acceleration.

Figure 6.8: Acceleration data for frequency 30 Hz, crank arm 3 mm, 1 kg payload.

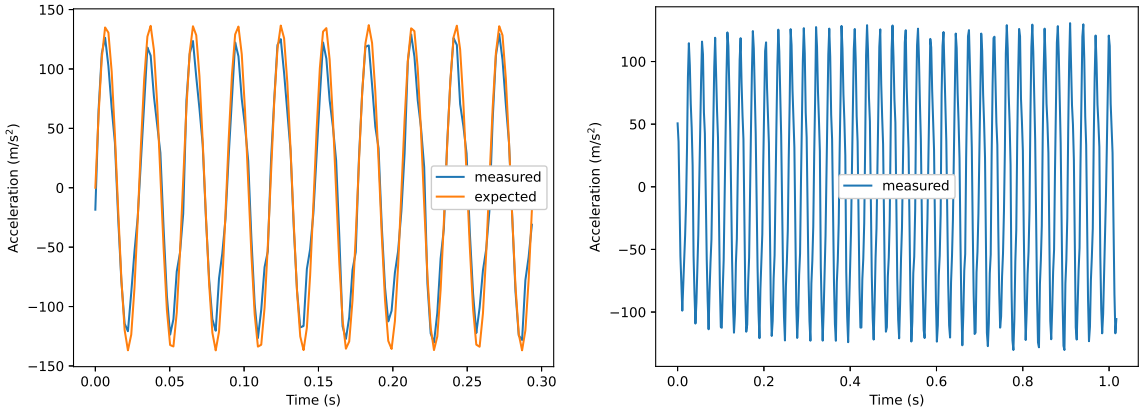

(a) Measured vs. expected comparison. **(b)** Measured acceleration.

Figure 6.9: Acceleration data for frequency 34 Hz, crank arm 3 mm, 1 kg payload.

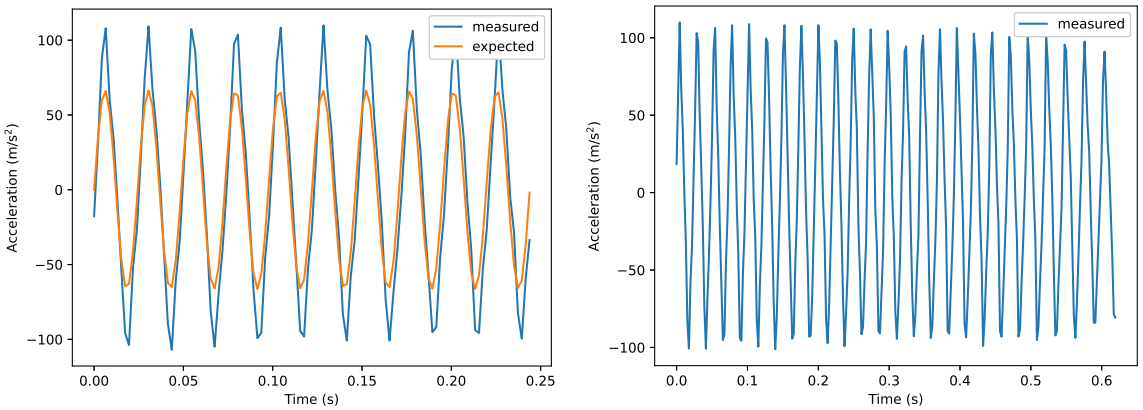

(a) Measured vs. expected comparison. **(b)** Measured acceleration.

Figure 6.10: Acceleration data for frequency 41 Hz, crank arm 1 mm, 1 kg payload.

The following table compares the average measured peak acceleration of the vibration against the expected acceleration for the vibration tests with the 1kg payload, similar to Table 6.2.

Freq. (Hz)	**Arm (mm)**	**Expected Peak (m/s^2)**	**Meas. Avg. Peak (m/s^2)**	**St. Dev. (m/s^2)**	**% Error**
5	3	2.96	8.50	0.08	+187.2
	5	4.93	11.11	0.36	+125.2
	6	5.92	11.03	0.28	+86.3
10	1	3.95	10.91	0.31	+176.4
	3	11.84	20.50	0.75	+73.2
	5	19.74	27.24	0.72	+38.0
	6	23.69	31.78	0.87	+34.2
15	1	8.88	17.51	1.03	+97.1
	3	26.62	36.89	0.71	+38.6
	5	44.41	43.22	1.25	−2.7
	6	53.29	57.05	1.31	+7.1
20	1	15.79	26.87	0.37	+70.1
	3	47.37	51.02	1.92	+7.7
	5	78.96	73.45	2.03	−7.0
25	3	74.01	72.22	1.36	−2.4
30	3	106.57	93.12	1.61	−12.6
34	3	136.91	124.22	3.52	−9.3
35	3	145.07	120.12	3.68	−17.2
40	1	63.16	94.37	2.39	+49.4
41	1	66.36	107.30	2.20	+61.7

Table 6.3: Average measured peaks for each 1kg-payload vibration test compared to the expected peaks.

6.4 Discussion

6.4.1 General Observations

From the qualitative and quantitative analysis in the previous section, we can make several general observations about the performance of the shaker table.

1. **The measured and expected frequencies align** in all the tests as seen from the graphs. This seems rather obvious since the frequency is directly related to the motor speed. If the motor is not overloaded, it should be able to drive the shaker table at the given frequency. This observation suggests that the motor is able to drive the shaker table at the given speeds with no issues.

2. **The acceleration peaks reach a consistent height**, as can be seen in both the graphs and the small standard deviation between peaks. This is also obvious since the acceleration depends on the position of the shaker table, which depends on the length of the crank arm, which is kept consistent for each test. This observation confirms that the shaker table's position is moving a consistent amount for each cycle.

3. **For smaller crank arm lengths (mostly 1 mm and 3 mm), the measured peak acceleration tends to be higher than the expected acceleration** as seen in the graphs. This is an unintended consequence, and we hypothesize it is most likely due to the free-fit oversize of the crank rod around the shoulder screws as described in Section 5.2. The extra space between the shoulder and the shaft hole causes the shaker table to be abruptly "jerked" to a higher acceleration peak at the ends at each cycle, so we see an additional acceleration at the peaks. The additional acceleration can be clearly seen in some of the graphs, such as in Figures D.4 and D.21.

   The amount of additional acceleration varies based on frequency, crank arm length, and payload mass. In general, when these quantities increase, the additional acceleration also increases. The presence of this additional acceleration also causes large percentage errors for some of the tests, especially for small crank arm lengths. However, this issue could be fixed by implementing a tighter tolerance on the crank rod shaft holes than the free fit in our prototype.

4. Assuming that the additional acceleration is indeed due to the free-fit oversize of the crank rod, **if we discount this acceleration, then the measured**

acceleration seems to match the expected acceleration for loads less than about 7 g (or about 70 m/s^2) in the qualitative graphs. Except for the sharp peaks in the graphs due to the additional acceleration, the plots of the measured acceleration are close to the plots of the expected acceleration. **However, when the loads increase past about 8g, we see that the measured acceleration tends to drop relative to the expected acceleration**, both for the no payload and the 1 kg payload tests. Interestingly enough, the discrepancy seems to be larger for the no-payload data than the 1 kg-payload data.

This discrepancy could have several causes. One possible explanation is that the shaker table is simply not able to reach such accelerations, or the performance starts to fall at high loads. However, this seems unlikely, since we can see from Table 6.3 that the shaker table acceleration was measured up to 124.22 m/s^2 at 34 Hz with a 3 mm crank arm length and 1 kg payload.

Another possible explanation is that the IMU we are using is not able to capture such high loads at high frequencies. We set the IMU to capture at 1 kHz, but it is unknown if this capture speed works for transient loads (such as high-frequency vibration) as well as quasi-static loads. However, looking at our graphs, the IMU seems to be able to capture the acceleration at up to 41 Hz, so this explanation may not be complete either.

A third explanation may come from deficiencies in the physical system. At the moment, we are still using 3D-printed motor and stage mounts, which are not as secure as machined aluminum mounts would be. Additionally, while testing, we noticed that the entire system would vibrate during high loads when the 1 kg payload mass was attached. This additional vibration displaces the breadboard (and thus the whole shaker table system) relative to the inertial frame, which changes the absolute dislacement of the IMu in the inertial frame. This may have resulted in the "damping" of the vibration profile we saw in the measured acceleration data.

Further testing is required to determine which of these reasons (if any) is why the performance of the shaker table does not exactly match the expected performance. To remove some uncertainty, we could procure a higher-quality IMU or attach the system to a heavier breadboard to prevent the system from vibrating. Unfortunately, the short time frame of this project prevented us from exploring this further.

5. **The design concept of this motorized shaker table can create predictable vibration in the range of vibration profiles required for CubeSats.** Although the current prototype of this design cannot encompass the full vibration requirements (discussed more in the following section), the vibration that this system creates generally matches what we could expect. A more powerful motor may be required to reach higher loads, but anyone wishing to use this design can upgrade (or downgrade) their motor appropriately according to their budget to achieve the loads they need. However, this system may not be suitable for precise vibration testing where the vibration levels must be very close to the vibration profile.

6.4.2 Verification of Vibration Profile

Table 6.4 shows the vibration profile from our requirements and compares it to the vibration profiles we were able to achieve without the payload and with the 1 kg payload.

No Payload			
Freq. (Hz)	**Accel. Requirement (g)**	**Achieved Accel. (g)**	**% Diff.**
5	0.60	1.11	+84.1
30	10.88	7.48	−31.1
34	13.97	9.25	−33.6
41	6.77	5.05	−25.3
1 kg Payload			
Freq. (Hz)	**Accel. Requirement (g)**	**Achieved Accel. (g)**	**% Diff.**
5	0.60	11.03	+1740
30	10.88	9.49	−12.6
34	13.97	12.66	−10.3
41	6.77	10.94	+61.6

Table 6.4: Comparison of achieved vibration to vibration requirements.

We can see that we were able to achieve the vibration requirements in the low and high frequency/load ranges, but we were not able to achieve the requirements in the mid frequency/load ranges.

For the range in which we overachieved the acceleration requirement, note that any payload that can survive a higher load (e.g. 1.11 g) than the requirement (e.g. 0.60 g) should also survive the required load. Thus, the shaker table can be used for verifying vibration requirements for payloads in these ranges.

In the mid ranges, even though we did not achieve the acceleration requirement, we expect that this system would be able to achieve the requirements given a more powerful motor and/or a greater range of crank arm lengths. More powerful motors can achieve higher torques to drive the shaker table, and a larger range of crank arm lengths would enable us to reach higher loads. As mentioned previously, deficiencies in the physical system could also be preventing us from reaching the expected load, so fixing these issues may also bring the measured acceleration up to the expected acceleration.

However, as mentioned in Observation #5 in the previous section, we believe that this design is capable of producing the vibration profile requirement outlined above. We have demonstrated that the prototype as-is can withstand loads of 12 g. Though we have not tested the system to failure, we believe that with a more powerful motor, a higher range of loads can be achieved.

6.5 Verification of All Requirements

Table 6.5 below verifies if the prototype satisfies the system requirements specified in Table 2.1.

No.	Requirement	Satisfied?
1	The system shall be able to create the vibration levels defined in Table 1.1.	Partially (see Section 6.4.2)
2	The system shall sustain vibration for at least 1 minute.	Yes
3	The system shall support test articles up to 1 kg.	Yes
4	The system shall support test articles with a base up to 10 cm by 10 cm.	Yes
5	The system shall have a manufacturing cost of $1000 or less not including the motor and associated costs.	Yes (see Appendix C.2)
6	The system shall be able to be powered by a typical 120 V wall outlet.	Yes
7	The system shall be be constructed of common materials and should be manufactured without special equipment.	Yes

Table 6.5: Verification of project requirements.

Our current prototype satisfies all project requirements besides the vibration profile (Requirement #1). However, as described in Section 6.4.2, we believe that an upgraded motor will allow the system to satisfy the vibration profile requirement.

Chapter 7

Conclusions

7.1 Summary

This report described the design, build, and test of a simple motorized CubeSat-scale shaker table. The design process included a trade study for the general design concept, COTS components selection, and custom component design. Building the system involved two prototypes: a 3D-printed prototype for initial proof-of-concept, and a machined prototype for testing and analysis. Finally, we tested the second prototype across a range of frequencies and loads to determine if it could match the requirements.

We concluded that although the current system cannot entirely satisfy the vibration profile we originally proposed, it is readily viable that the a motorized shaker table system could create the vibration profile given an upgraded motor and some minor changes to the design. Additionally, the system does satisfy the other requirements we set out.

7.2 Future Work

Given that this was a short 12-week project, there are some improvements that we did not have time to implement. Future work on this project could adopt the following suggestions to make a more robust, capable shaker table system.

7.2.1 Upgrade Motor

As mentioned previously, future users of this system can upgrade the motor to a motor with higher maximum speed and torque to fit different vibration profiles. For instance, original vibration profile we referenced in Table 2.3 would require a higher-torque motor to achieve the 22 g load.

7.2.2 Additional Eccentric Shaft Hubs

The eccentric shaft hub design provides users with the flexibility to create their own vibration profiles. Our eccentric shaft hub included amplitude options of 1 mm, 3 mm, 5 mm, and 6 mm. While this satisfied some of the vibration profile we originally required, users can machine additional eccentric shaft hubs to satisfy different vibration profiles.

For instance, a user may want to sweep a frequency range and induce the same vibration load at every frequency, such as the following profile:

ω **(Hz)**	ω **(rad/s)**	$a_{\mathbf{max}}$ **(g)**	$a_{\mathbf{max}}$**(m/s^2)**	r **(mm)**	$F_{\mathbf{max}}$ **(N)**	τ **(Nm)**
10	62.83	5	49.05	12.42	56.41	0.701
15	94.25	5	49.05	5.00	56.41	0.282
20	125.66	5	49.05	3.11	56.41	0.175
25	157.08	5	49.05	1.99	56.41	0.112
30	188.50	5	49.05	1.38	56.41	0.078
35	219.91	5	49.05	1.01	56.41	0.057
40	251.33	5	49.05	0.78	56.41	0.044
45	282.74	5	49.05	0.61	56.41	0.035
50	314.16	5	49.05	0.50	56.41	0.028

Table 7.1: Amplitude, force, and torque calculations for sample vibration profile with constant load of 5 g at multiple frequencies.

The crank arm lengths r range from 12.42 mm to 0.50 mm. These are feasible lengths to machine onto 2-3 eccentric shaft hubs, and users can swap out hubs to achieve the full vibration profile.

7.2.3 Tighter Tolerance on Crank Rod

As described in Section 6.4.1, the "jiggle" of the crank rod may cause additional acceleration, causing loads to be higher than predicted. To remedy this, the crank rod should be re-machined with a tighter tolerance. We designed the shaft holes to have a diameter of 5.25 mm to have a close fit around a 5 mm shoulder screw. However, we suggest an even tighter tolerance of 5.10 mm to reduce the additional acceleration experienced by the linear stage. If the user chooses to outsource the machining of this part, this tighter tolerance may result in higher costs.

7.2.4 Replace Shoulder Screws with Bearings

As mentioned in Section 4.1, we could replace the shoulder screws in the current design with roller bearings to reduce friction between the shoulder screw and crank rod shaft hole. One such crank rod design is shown below. The bearings are inset around the shaft holes.

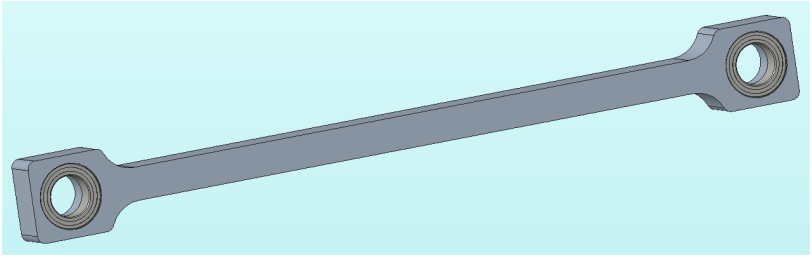

Figure 7.1: Crank rod with bearings in shaft holes.

7.2.5 Low-Friction Linear Stage

At higher frequencies (up to 100 Hz) and as the system experiences increased wear and tear, we might expect the linear stage crossed-roller bearings to degrade as dust and debris accumulate. While we can increase the lifespan of our linear stage by adding lubrication, an alternative is to redesign the linear stage without any traditional bearings. Instead of bearings, we could consider a plain bearing manufactured out of low-friction material such as Teflon. This would reduce the weight of the moving stage, increasing the payload mass capacity.

Bibliography

[1] Aerospace Specification Metals, Inc. Aluminum 6061-t6; 6061-t651. https://asm.matweb.com/search/SpecificMaterial.asp?bassnum=ma6061t6.

[2] Applied Motion. TSM34Q-1AG - NEMA 34 StepSERVO Integrated Motor w/ Q Programming and Modbus RTU. https://www.applied-motion.com/products/stepservo-integrated-motors/tsm34q-1ag.

[3] CubeSat. CubeSat design sepcification, revision 13. https://static1.squarespace.com/static/5418c831e4b0fa4ecac1bacd/t/56e9b62337013b6c063a655a/1458157095454/cds_rev13_final2.pdf, Feb. 2014.

[4] enDAQ. Bernoulli-Euler beams. https://endaq.com/pages/bernoulli-euler-beams.

[5] M. Galvin. Qual test facilities. https://tigersats.princeton.edu/qual-test-facilities#ViAc.

[6] Lin Engineering. BL34E34-01 BLDC motor. https://www.linengineering.com/products/brushless-motors/standard-bldc-motors/bl34-series/bl34e34-01/BL34E34-01.

[7] NASA. General environmental verification standard (GEVS) for GSFC flight programs and projects. https://standards.nasa.gov/sites/default/files/standards/GSFC/B/0/gsfc-std-7000b_signature_cycle_04_28_2021_fixed_links.pdf, Apr. 2021.

[8] Optics Focus. Manual positioning stage. https://optics-focus.com/manual-positioning-stage-p-797.html?zenid=v7ter245iknp8rpacibuou1bg0.

[9] SpaceX. Falcon user's guide. https://www.spacex.com/media/falcon-users-guide-2021-09.pdf, Sept. 2021.

Appendix A

Reference Drawings

The following figures are reference drawings for the five machined parts: eccentric shaft hub, stage attachment, crank rod, motor mount, and stage mount.

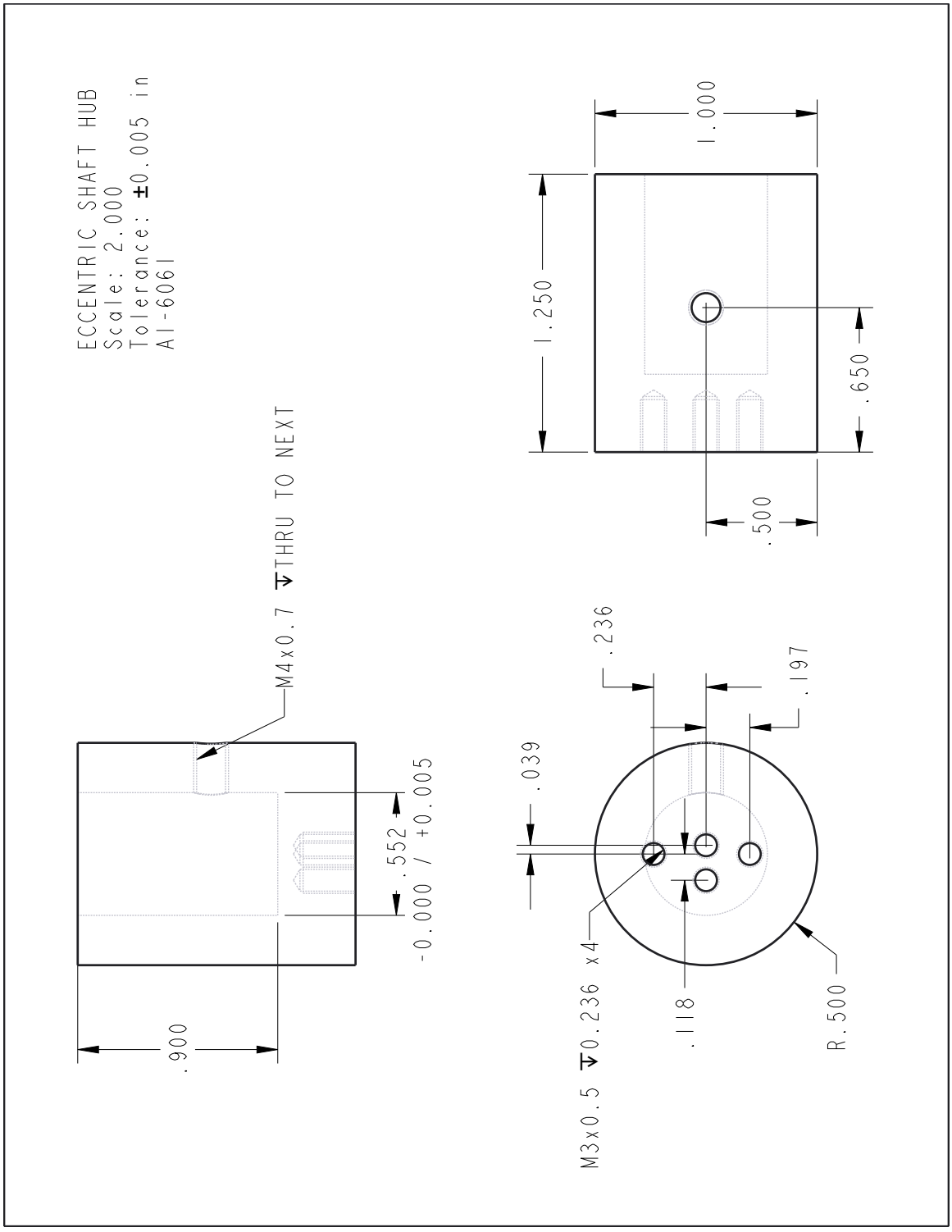

Figure A.1: Reference for eccentric shaft hub.

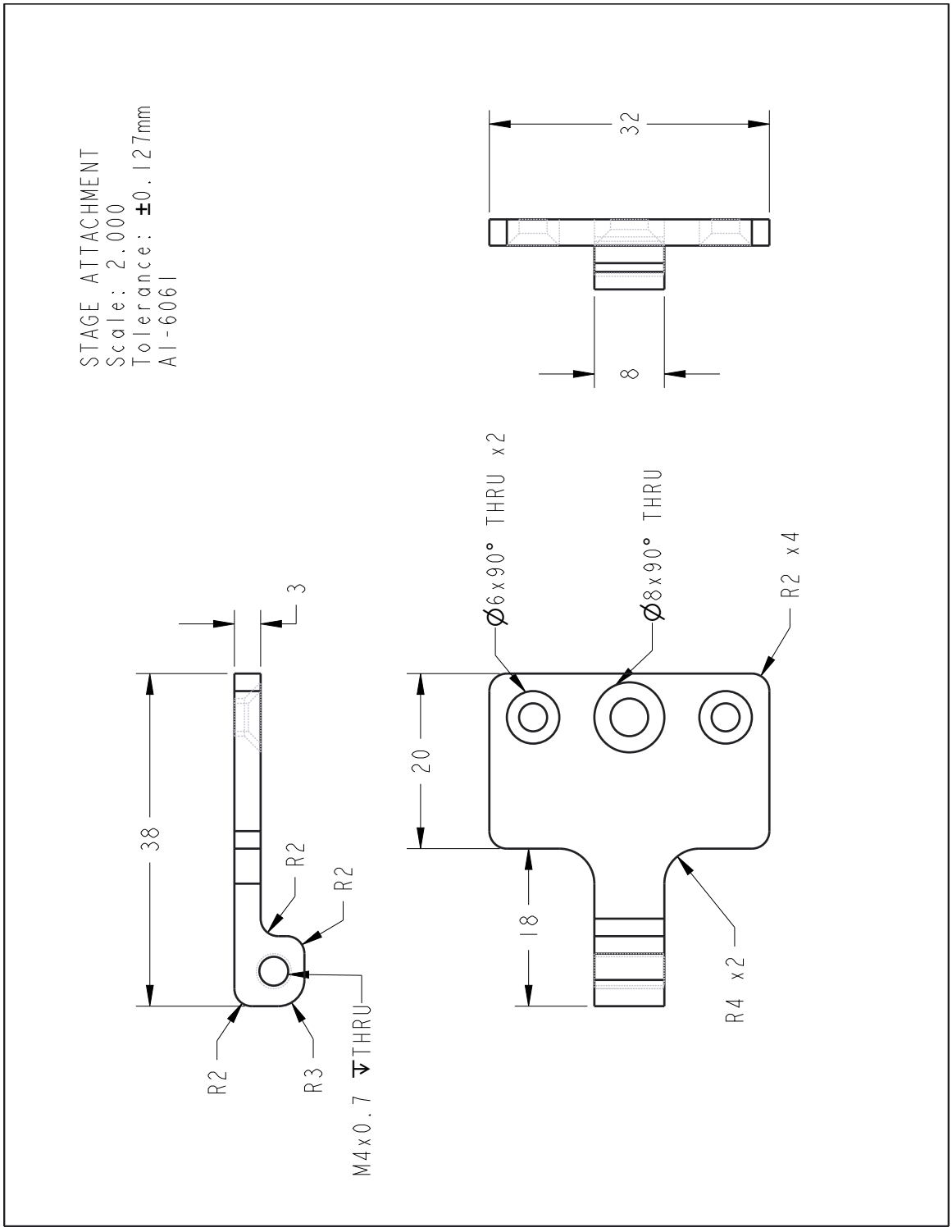

Figure A.2: Reference for stage attachment.

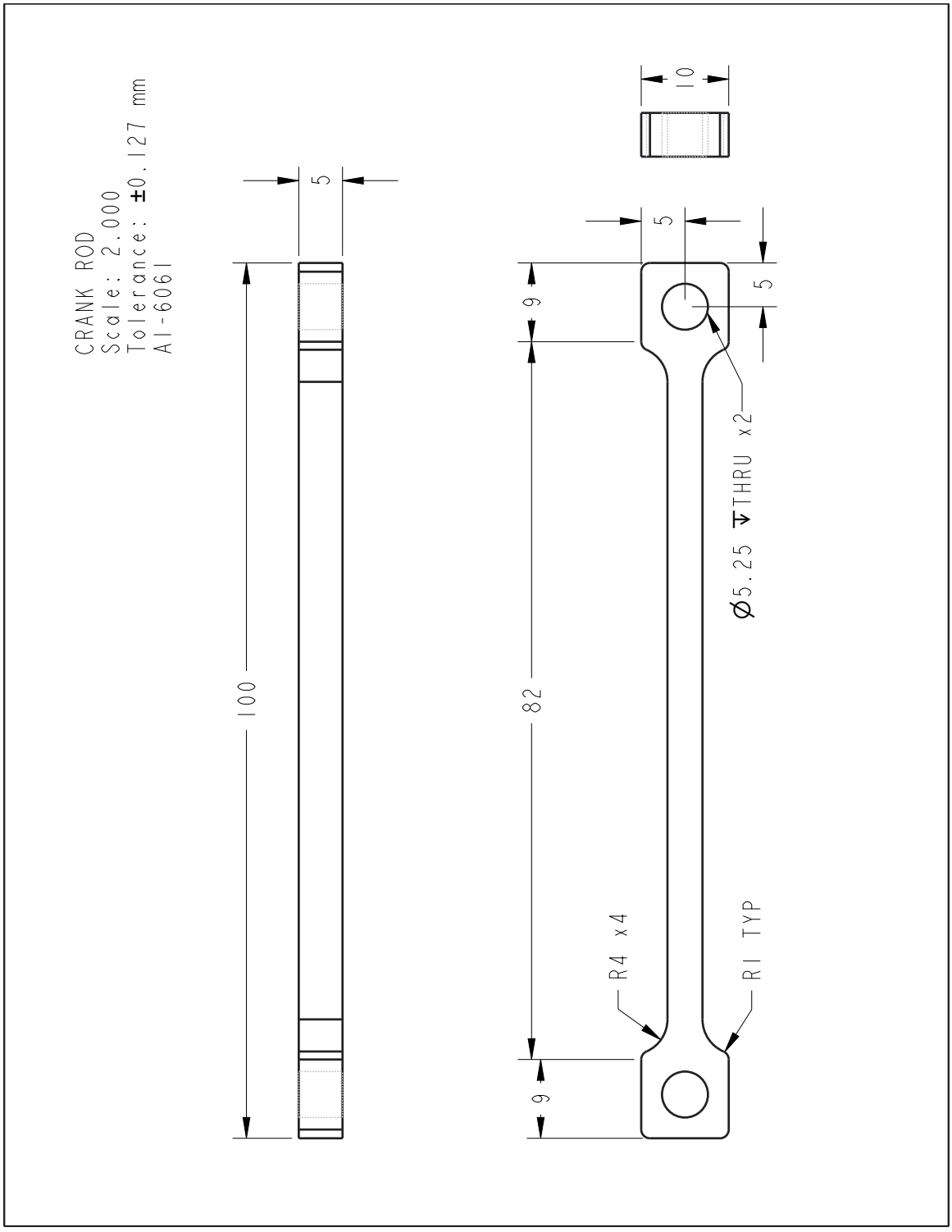

Figure A.3: Reference for crank rod.

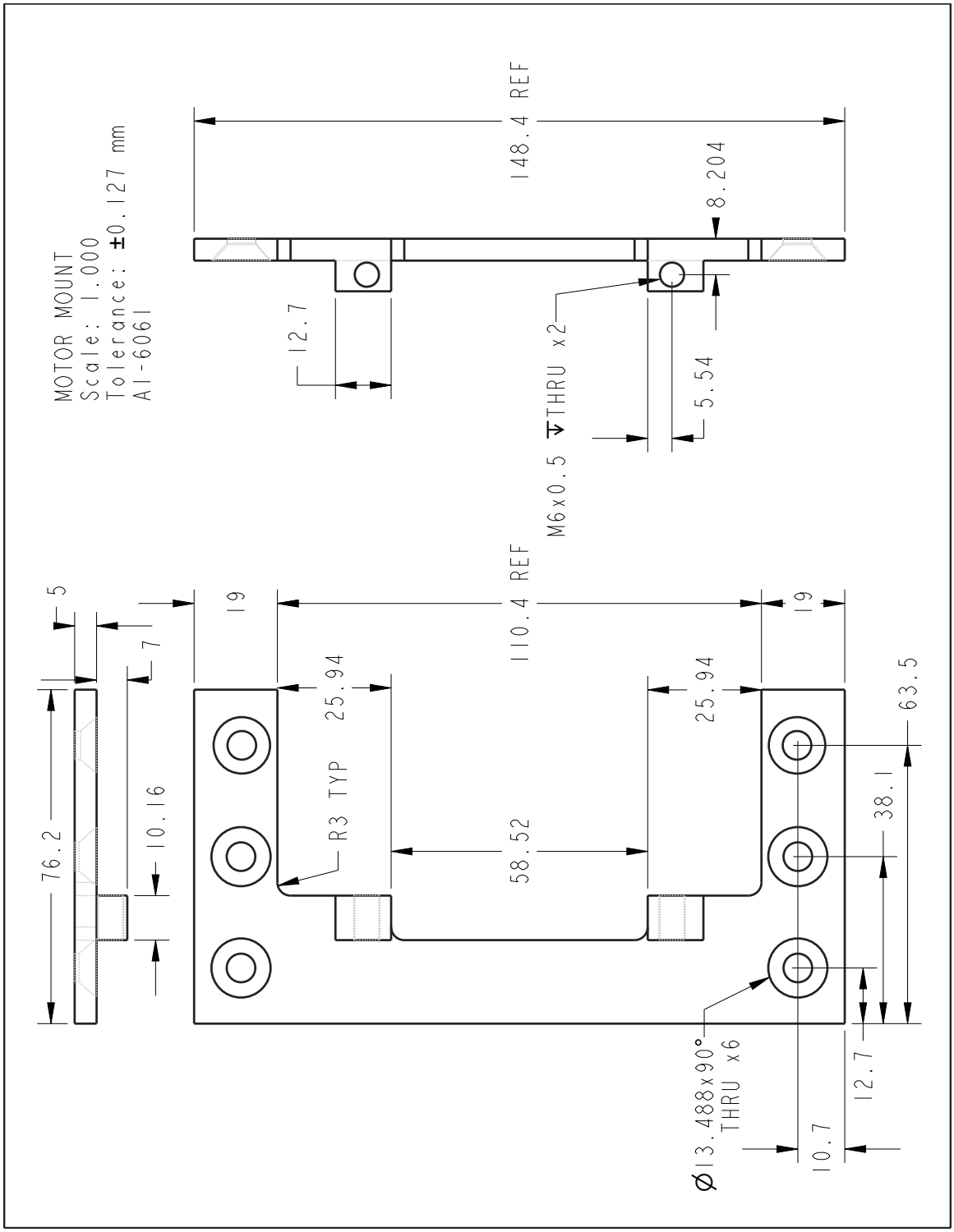

Figure A.4: Reference for motor mount.

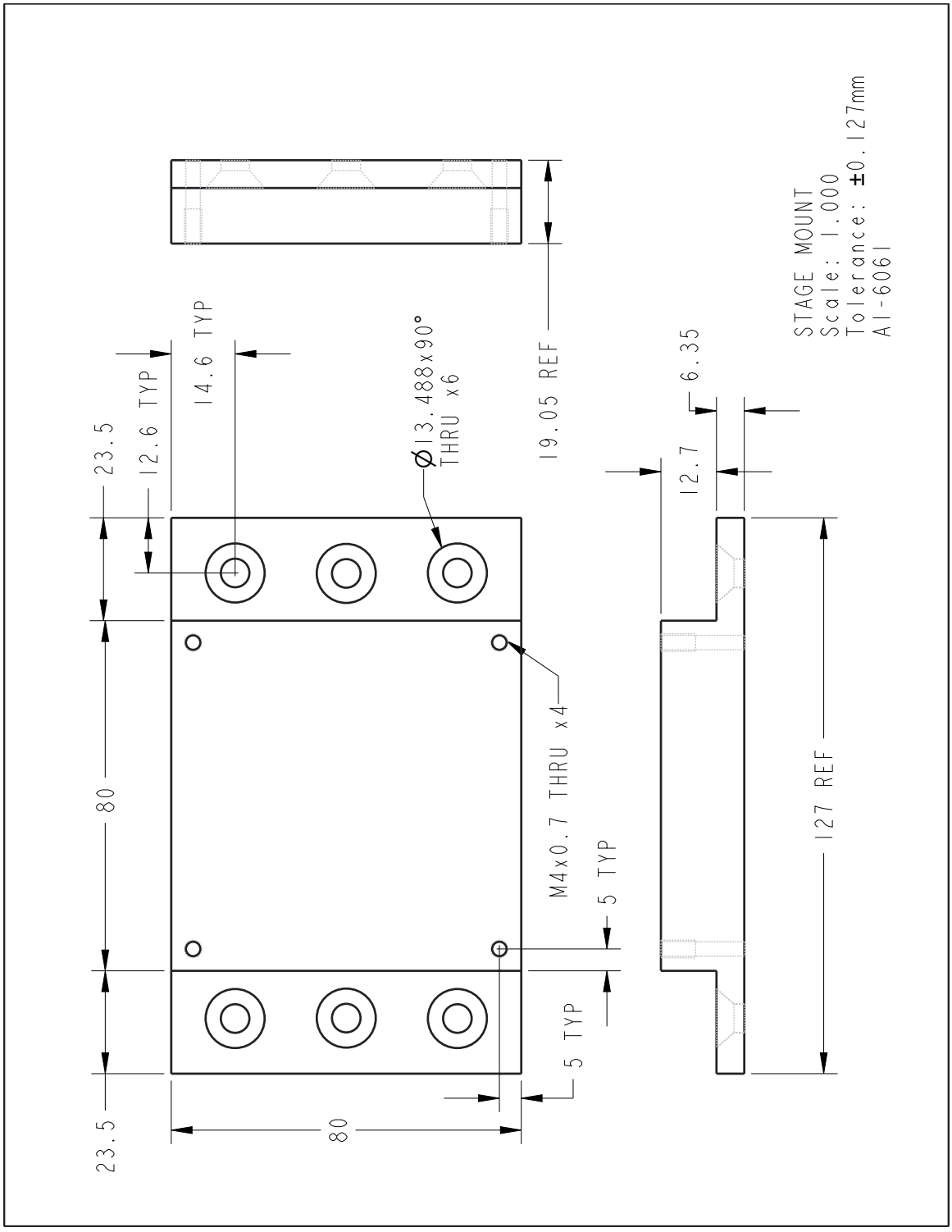

Figure A.5: Reference for stage mount.

Appendix B

Code

B.1 Data Collection via Arduino

The following code is modified from Bolder Flight System's example code for collecting data from a MPU-9250 IMU. This script extracts acceleration data from the IMU and prints it to Serial.

```
/*
Brian R Taylor
brian.taylor@bolderflight.com

Copyright (c) 2022 Bolder Flight Systems

Permission is hereby granted, free of charge, to any person obtaining a copy of this software
and associated documentation files (the "Software"), to deal in the Software without restriction,
including without limitation the rights to use, copy, modify, merge, publish, distribute,
sublicense, and/or sell copies of the Software, and to permit persons to whom the Software is
furnished to do so, subject to the following conditions:

The above copyright notice and this permission notice shall be included in all copies or
```

```
14 substantial portions of the Software.
15
16 THE SOFTWARE IS PROVIDED "AS IS", WITHOUT WARRANTY OF ANY KIND, EXPRESS
       OR IMPLIED, INCLUDING
17 BUT NOT LIMITED TO THE WARRANTIES OF MERCHANTABILITY, FITNESS FOR A
       PARTICULAR PURPOSE AND
18 NONINFRINGEMENT. IN NO EVENT SHALL THE AUTHORS OR COPYRIGHT HOLDERS BE
       LIABLE FOR ANY CLAIM,
19 DAMAGES OR OTHER LIABILITY, WHETHER IN AN ACTION OF CONTRACT, TORT OR
       OTHERWISE, ARISING FROM,
20 OUT OF OR IN CONNECTION WITH THE SOFTWARE OR THE USE OR OTHER DEALINGS
       IN THE SOFTWARE.
21 */
22
23 #include "MPU9250.h"
24
25 // an MPU9250 object with the MPU-9250 sensor on I2C bus 0 with address
       0x68
26 MPU9250 IMU(Wire,0x68);
27 int startup;
28 long t_start; // start time
29
30 void setup() {
31   Serial.begin(115200);
32   while(!Serial) {} // wait for Serial to start
33
34   // start communication with IMU
35   startup = IMU.begin();
36   if (startup < 0) {
37     Serial.println("Could not connect to IMU.");
38     Serial.print("Status: ");
39     Serial.println(startup);
40     while(1) {}
41   }
42
43   // set the accelerometer range to 16G
```

```
44   IMU.setAccelRange(MPU9250::ACCEL_RANGE_16G);
45   // set the bandwidth to 20 Hz
46   IMU.setDlpfBandwidth(MPU9250::DLPF_BANDWIDTH_20HZ);
47   // set the SRD to 0 for a 1000 Hz update rate
48   IMU.setSrd(0);
49
50   t_start = micros();
51 }
52
53 void loop() {
54   IMU.readSensor(); // get sensor readout
55
56   Serial.print(micros() - t_start);
57   Serial.print("\t");
58   Serial.println(IMU.getAccelX_mss(),6); // acceleration to 6 digits
59 }
```

B.2 Data Analysis via Python

The following code plots acceleration data and compares it to the expected acceleration. It also computes the average and standard deviation of the acceleration peaks.

```
import numpy as np
import matplotlib.pyplot as plt
import scipy.signal as signal

## plot vibration test data
freq = 20 # frequency (Hz)
arm = 1 # crank arm length (mm)
payload = 1 # 1 if no payload, 2 if payload

# load in data and unpack
values = np.loadtxt('clean-data/freq{}_arm{}_{}.txt'.format(freq, arm,
    payload))
t = values[:, 0] / 1e6 # convert microseconds to seconds
a = values[:, 1]

# find smaller range for analysis
min = 1250
max = -590
t = t[min:max]
a = a[min:max]

# shift initial time to 0 seconds
t = t - t[0]

# plot measured acceleration data
plt.plot(t, a, label='measured')

# calculate and plot expected acceleration
expected = arm / 1000 * (freq*2*np.pi)**2 * np.sin(2 * np.pi * freq * t
    + 0)
expected_max = np.max(expected)
plt.plot(t, expected, label='expected')
```

```
plt.legend()
plt.xlabel('Time (s)')
plt.ylabel('Acceleration (m/s$^2$)')
plt.savefig('freq{}_arm{}_{}_full.eps'.format(freq, arm, payload),
    bbox_inches='tight')
plt.show()

## analyze peak accelerations
# find peaks
t_peaks = signal.find_peaks(a, height=0, distance=10)[0] # indices of
    peaks
times = t[t_peaks] # time of peaks
peaks = a[t_peaks] # acceleration at peaks

# statistics
print('expected avg peak:', expected_max)
print('average peak:', np.mean(peaks))
print('standard deviation:', np.std(peaks))

# plot
plt.plot(t, a, label='acceleration data')
plt.scatter(times, peaks, c='r', label='peaks')
plt.xlabel('Time (s)')
plt.ylabel('Acceleration (m/s$^2$)')
plt.legend()
plt.savefig('peaks_freq{}_arm{}_{}.eps'.format(freq, arm, 1),
    bbox_inches='tight')
plt.show()
```

Appendix C

Budget and Bill of Materials

C.1 Budget

The following table itemizes all materials purchased for this project. The BLDC motor and motor controller were returned to Lin Engineering and reimbursed. Note that this project was granted $2,195.00 in funding. Some items, such as the MPU-9250 IMU, Arduino Uno, and 1/4-20 screws, were provided by the TigerSats Lab and thus did not count towards the project budget.

Item	PN	Supplier	Qty	Unit Price	Total Price
BLDC motor*	BL34E34-01D-05RO	Lin Engineering	1	$336.52	$336.52
BLDC motor controller*	BLDC100-BL34E34-01	Lin Engineering	1	$209.98	$209.98
48V 10A power supply	B08GFQZFC1	Drok	1	$39.99	$39.99
70V 6.7A power supply	PS480D72	Applied Motion	1	$458.00	$458.00
Linear stage	MAX-80C-25	Optics Focus	1	$83.00	$83.00
Eccentric shaft hub	N/A	Xometry	1	$214	$213.61
Stage attachment	N/A	Xometry	1	$202	$202.26
Crank rod,	N/A	Xometry	1	$134	$133.61
1kg brass block	N/A	Xometry	1	$239	$239.00
M2 shoulder screw	90265A111	McMaster-Carr	5	$2.55	$12.75
M4 set screw, soft tip	93285A131	McMaster-Carr	1	$14.02	$14.02
M4 heat-set inserts, long	94459A160	McMaster-Carr	1	$13.89	$13.89
M4 nylon patch screws	93705A823	McMaster-Carr	1	$6.21	$6.21
M4 shoulder screws	90278A321	McMaster-Carr	5	$4.26	$21.30
M3 shoulder screws	90265A188	McMaster-Carr	3	$7.20	$21.60
M3 flathead screws, pack of 100	92125A130	McMaster-Carr	1	$7.31	$7.31
M4 flathead screws, pack of 100	92125A190	McMaster-Carr	1	$9.50	$9.50
M3 shoulder screw, 5mm OD, 6mm length	90265A189	McMaster-Carr	1	$8.40	$8.40
M3 shoulder screw, 5mm OD, 7mm shoulder	90265A192	McMaster-Carr	1	$9.20	$9.20
M4 shoulder screw, 5mm OD, 6mm shoulder	90265A127	McMaster-Carr	1	$5.04	$5.04
M4 shoulder screw, 5mm OD, 7mm shoulder	90278A503	McMaster-Carr	1	$7.67	$7.67
				Total	**$2,052.86**
				Total (without returned items)	**$1,506.36**

Table C.1: Project budget.
*Returned item.

C.2 Bill of Materials

The materials required to build a machined prototype of the shaker table system are shown below. Note that the prices for all machined parts are for "Economy" speed (4 business days) and that these prices are subject to change. Shipping is not included.

Item	**PN**	**Supplier**	**Qty**	**Unit Price**	**Total Price**
StepSERVO motor and driver	TSM34Q-1AG	Applied Motion	1	$785.00	$785.00
Power supply	PS480D72	Applied Motion	1	$458.00	$458.00
Linear stage	MAX-80C-25	Optics Focus	1	$83.00	$83.00
Arduino Uno	A000066	Arduino	1	$30.18	$30.18
IMU	MPU-9250	SunFounder	1	$11.95	$11.95
Crank rod, machined	N/A	Xometry	1	$113.51	$113.51
Eccentric shaft hub, machined	N/A	Xometry	1	$185.87	$185.87
Table attachment, machined	N/A	Xometry	1	$174.12	$174.12
Motor mount, machined	N/A	Xometry	1	$196.67	$196.67
Table mount, machined	N/A	Xometry	1	$160.98	$160.98
M3 shoulder screw, 5mm diameter, 6mm shoulder	90265A189	McMaster-Carr	1	$8.40	$8.40
M4 shoulder screw, 5mm diameter, 6mm shoulder	90265A127	McMaster-Carr	1	$5.04	$5.04
M3 flathead screws, 8 mm length	92125A130	McMaster-Carr	1	$7.31	$7.31
M4 flathead screws, 8 mm length	92125A190	McMaster-Carr	1	$9.50	$9.50
1/4-20 flathead screws, 7/8" length, pack of 25	92210A541	McMaster-Carr	1	$6.16	$6.16
				Total (without motor, power supply)	**$992.69**
				Total (with motor, power supply)	**$2235.69**

Table C.2: Bill of materials.

Appendix D

Additional Acceleration Data

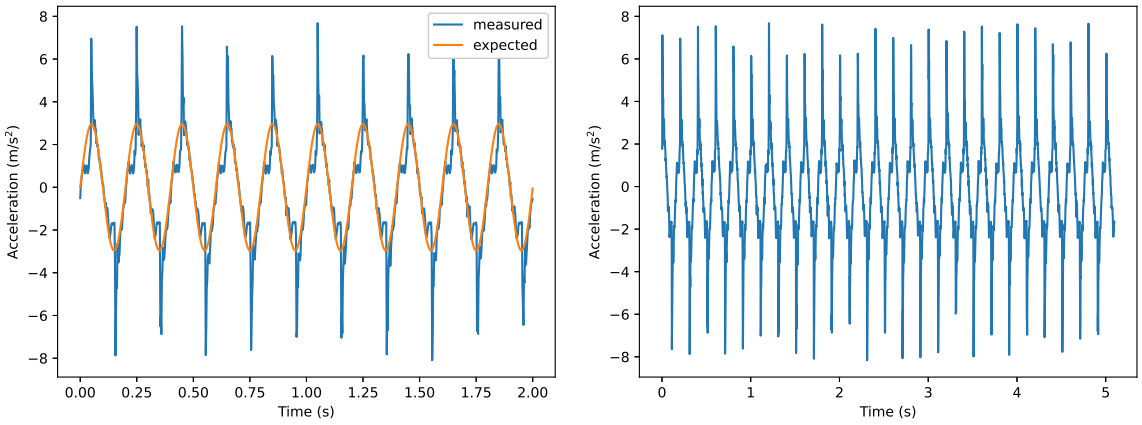

(a) Measured vs. expected comparison. **(b)** Measured acceleration.

Figure D.1: Acceleration data for frequency 5 Hz, crank arm 3 mm, no payload.

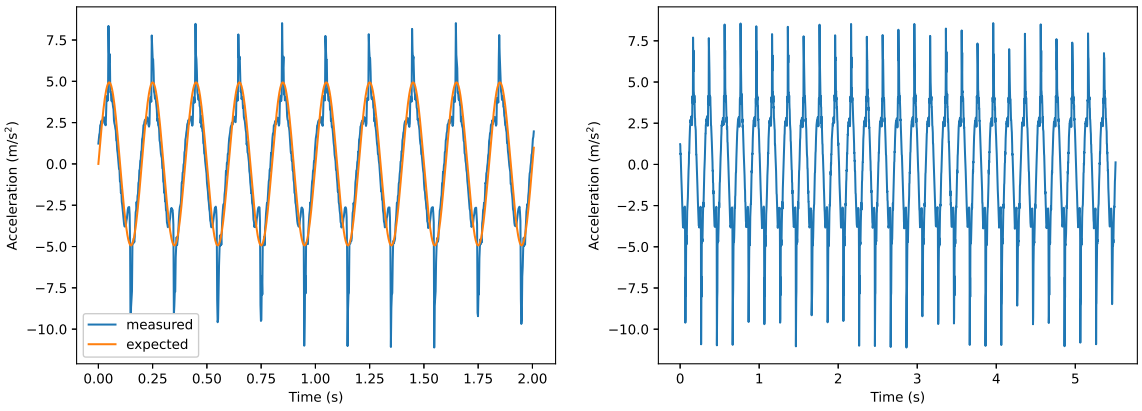

(a) Measured vs. expected comparison. **(b)** Measured acceleration.

Figure D.2: Acceleration data for frequency 5 Hz, crank arm 5 mm, no payload.

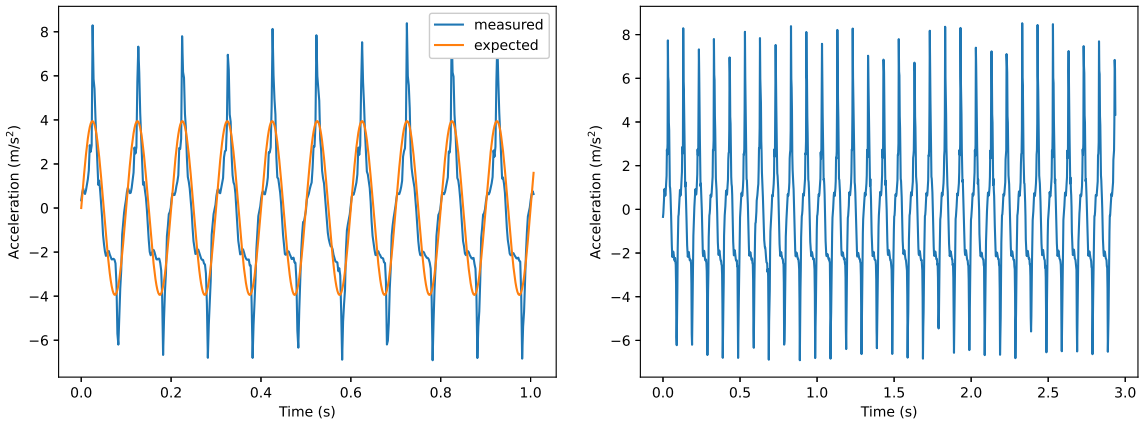

(a) Measured vs. expected comparison. **(b)** Measured acceleration.

Figure D.3: Acceleration data for frequency 10 Hz, crank arm 1 mm, no payload.

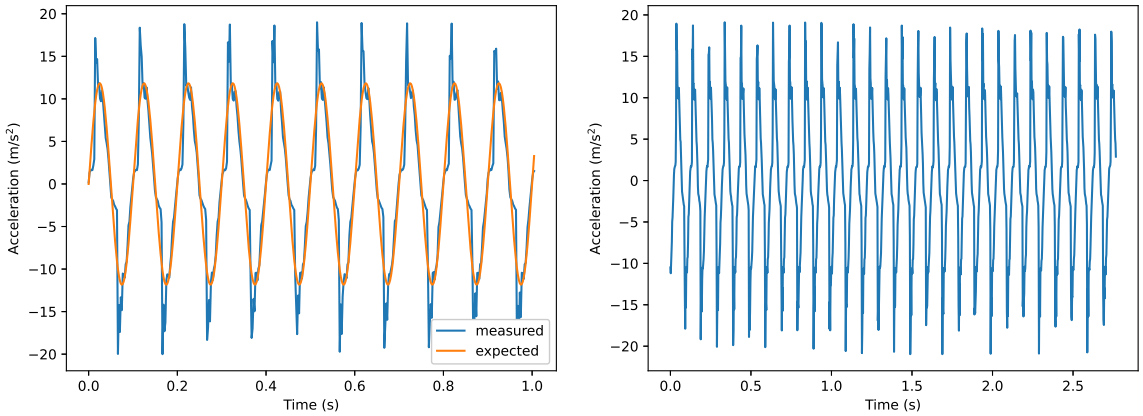

(a) Measured vs. expected comparison. **(b)** Measured acceleration.

Figure D.4: Acceleration data for frequency 10 Hz, crank arm 3 mm, no payload.

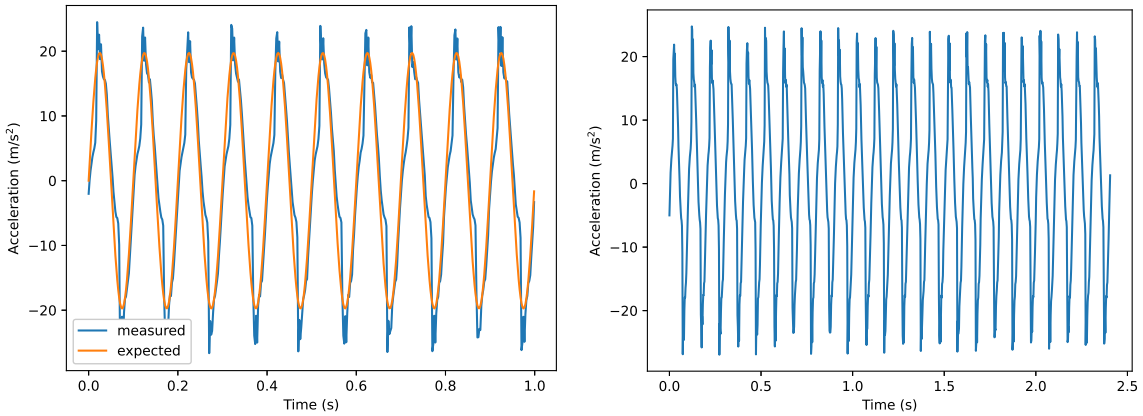

(a) Measured vs. expected comparison. **(b)** Measured acceleration.

Figure D.5: Acceleration data for frequency 10 Hz, crank arm 5 mm, no payload.

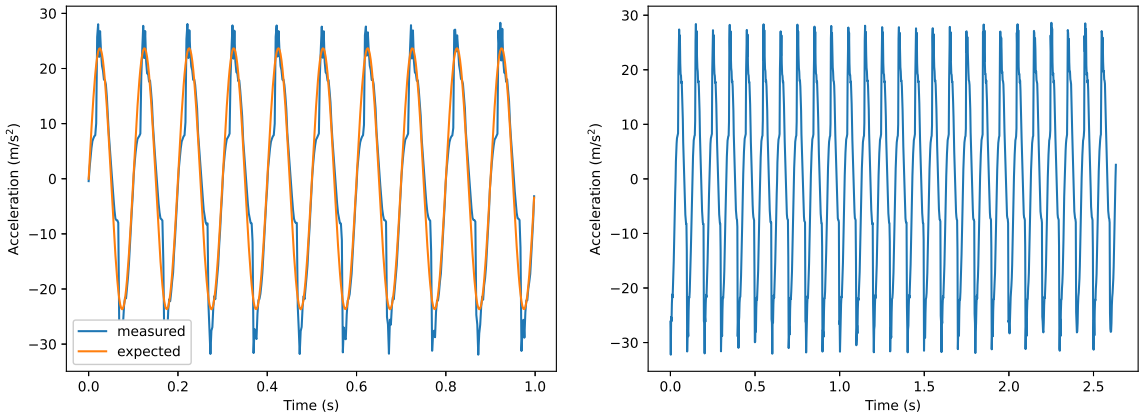

(a) Measured vs. expected comparison. **(b)** Measured acceleration.

Figure D.6: Acceleration data for frequency 10 Hz, crank arm 6 mm, no payload.

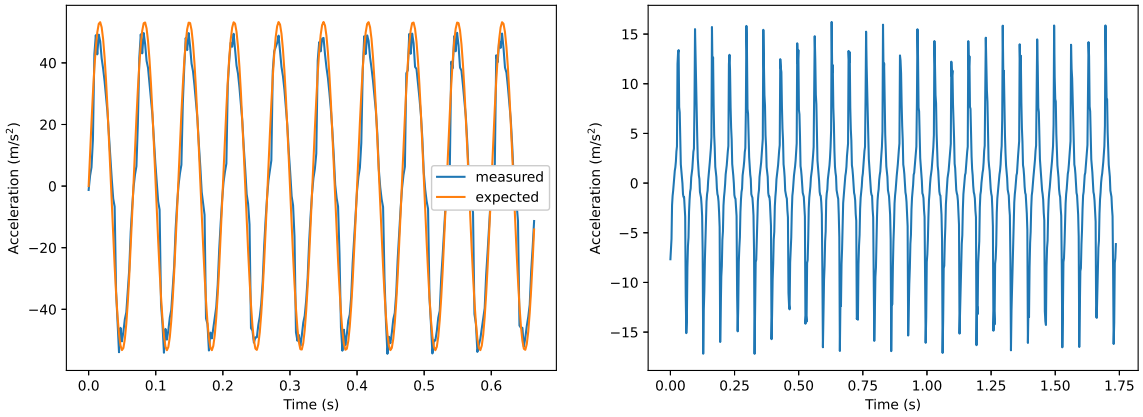

(a) Measured vs. expected comparison. **(b)** Measured acceleration.

Figure D.7: Acceleration data for frequency 15 Hz, crank arm 1 mm, no payload.

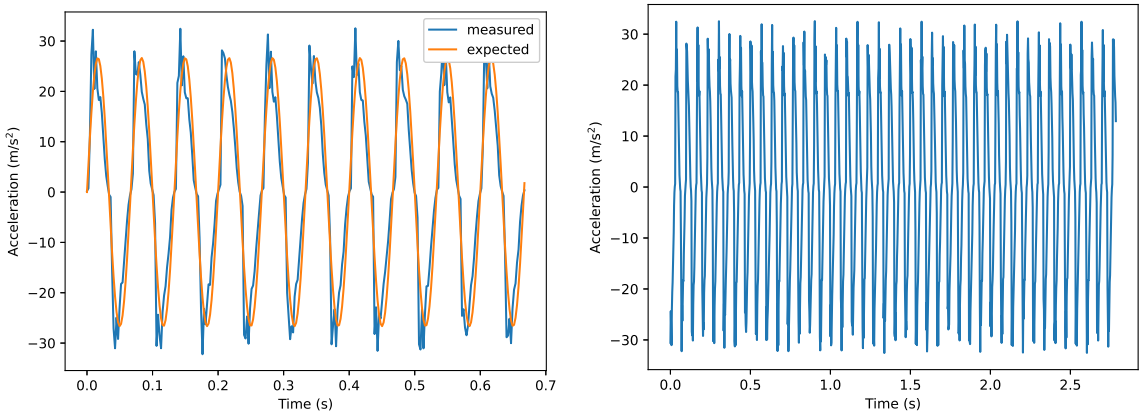

(a) Measured vs. expected comparison. **(b)** Measured acceleration.

Figure D.8: Acceleration data for frequency 15 Hz, crank arm 3 mm, no payload.

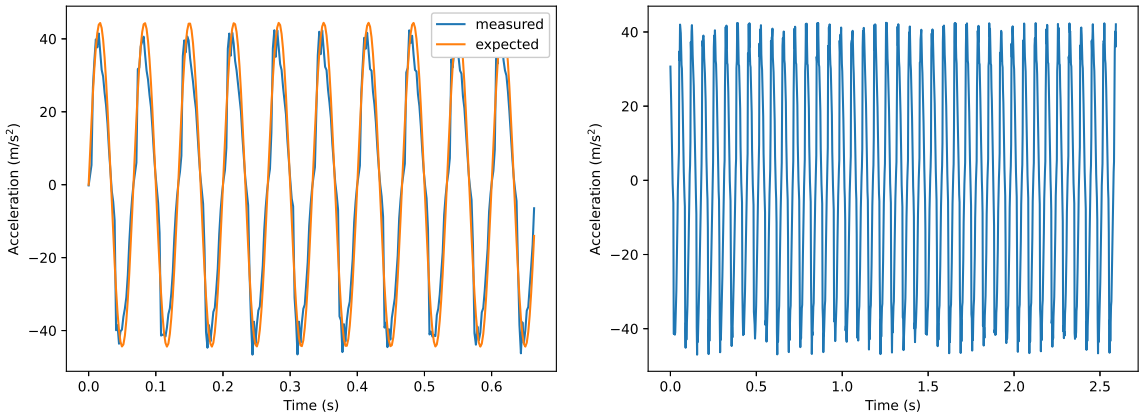

(a) Measured vs. expected comparison. **(b)** Measured acceleration.

Figure D.9: Acceleration data for frequency 15 Hz, crank arm 5 mm, no payload.

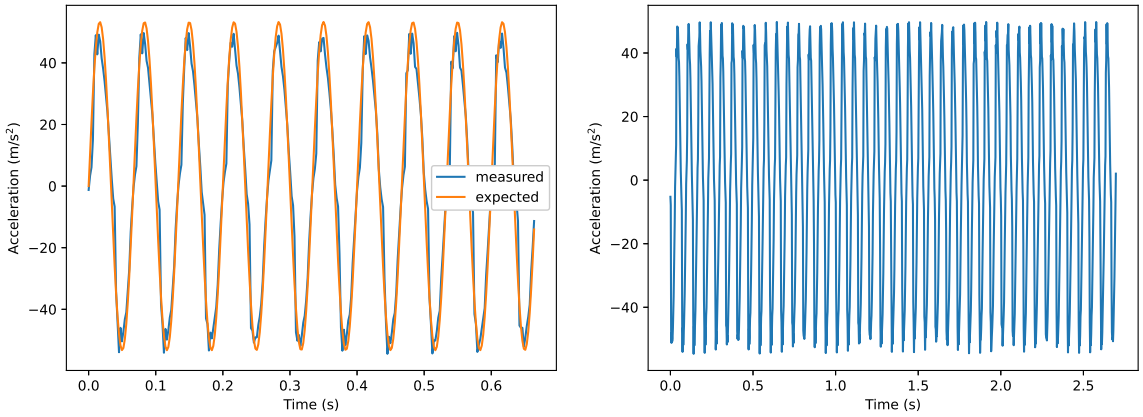

(a) Measured vs. expected comparison. **(b)** Measured acceleration.

Figure D.10: Acceleration data for frequency 15 Hz, crank arm 6 mm, no payload.

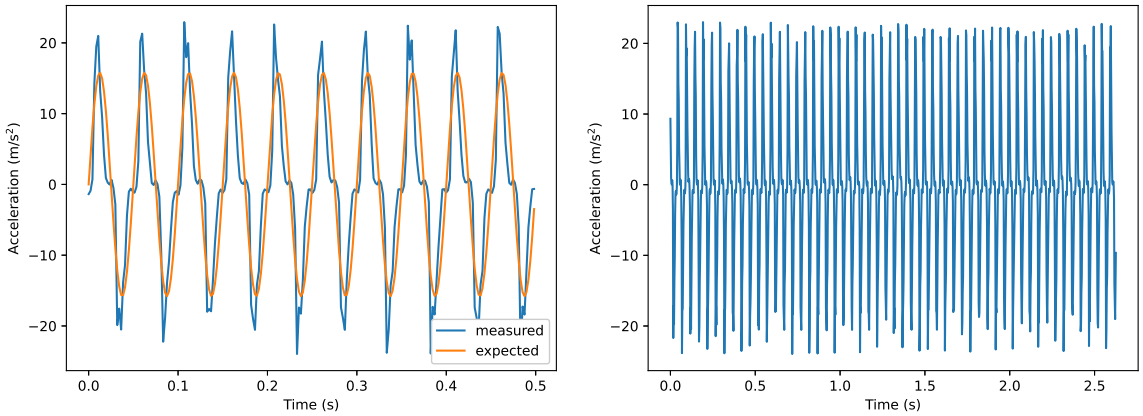

(a) Measured vs. expected comparison. **(b)** Measured acceleration.

Figure D.11: Acceleration data for frequency 20 Hz, crank arm 1 mm, no payload.

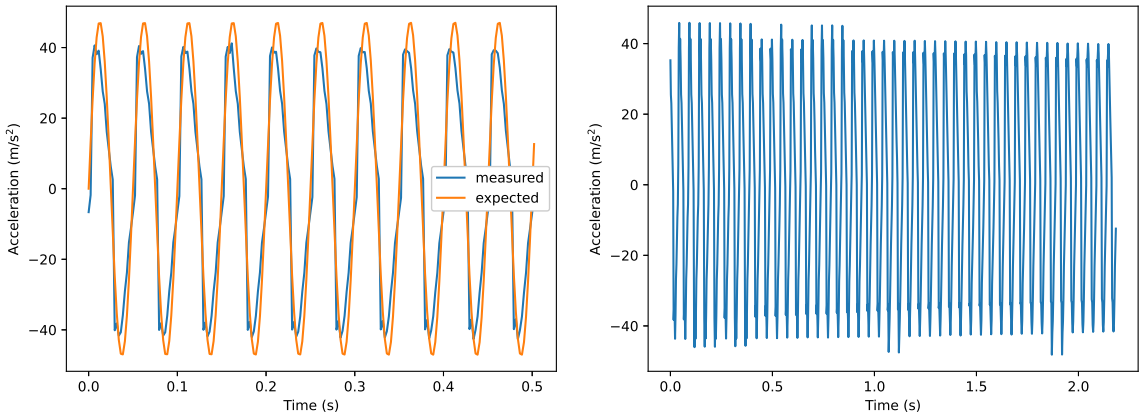

(a) Measured vs. expected comparison. **(b)** Measured acceleration.

Figure D.12: Acceleration data for frequency 20 Hz, crank arm 3 mm, no payload.

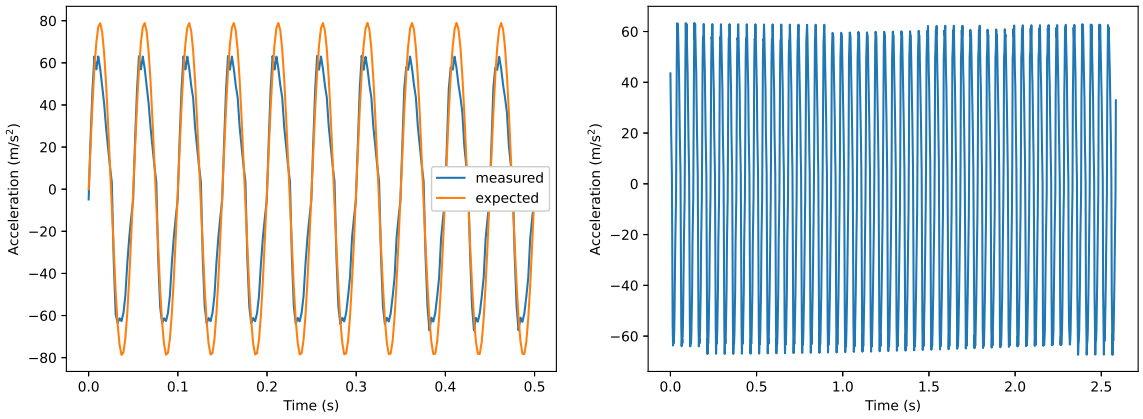

(a) Measured vs. expected comparison. **(b)** Measured acceleration.

Figure D.13: Acceleration data for frequency 20 Hz, crank arm 5 mm, no payload.

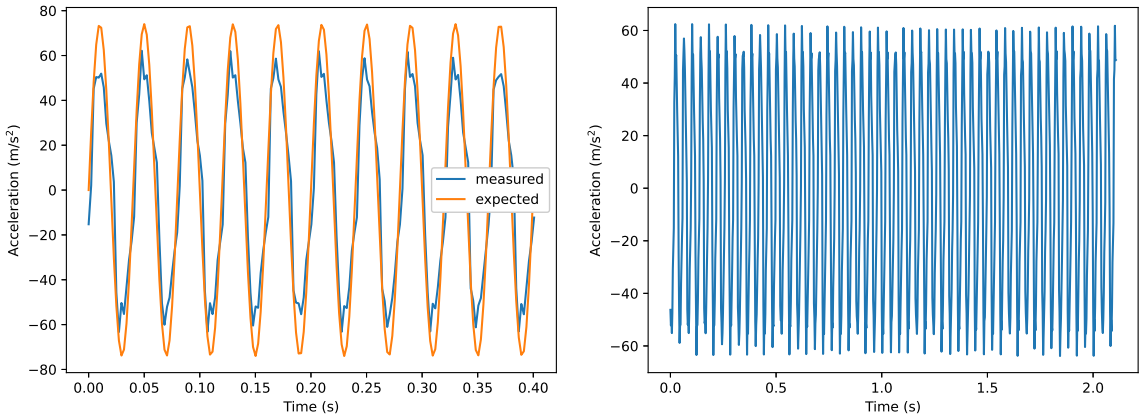

(a) Measured vs. expected comparison. **(b)** Measured acceleration.

Figure D.14: Acceleration data for frequency 25 Hz, crank arm 3 mm, no payload.

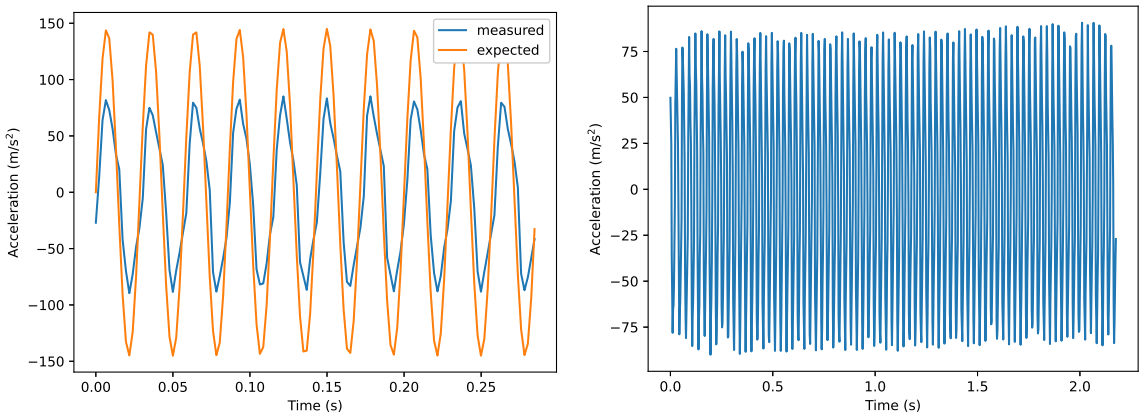

(a) Measured vs. expected comparison. **(b)** Measured acceleration.

Figure D.15: Acceleration data for frequency 35 Hz, crank arm 3 mm, no payload.

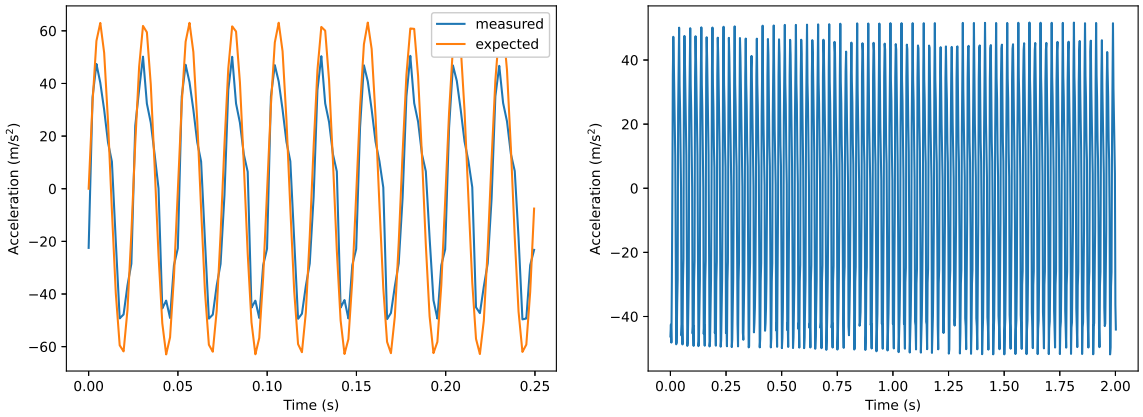

(a) Measured vs. expected comparison. **(b)** Measured acceleration.

Figure D.16: Acceleration data for frequency 40 Hz, crank arm 1 mm, no payload.

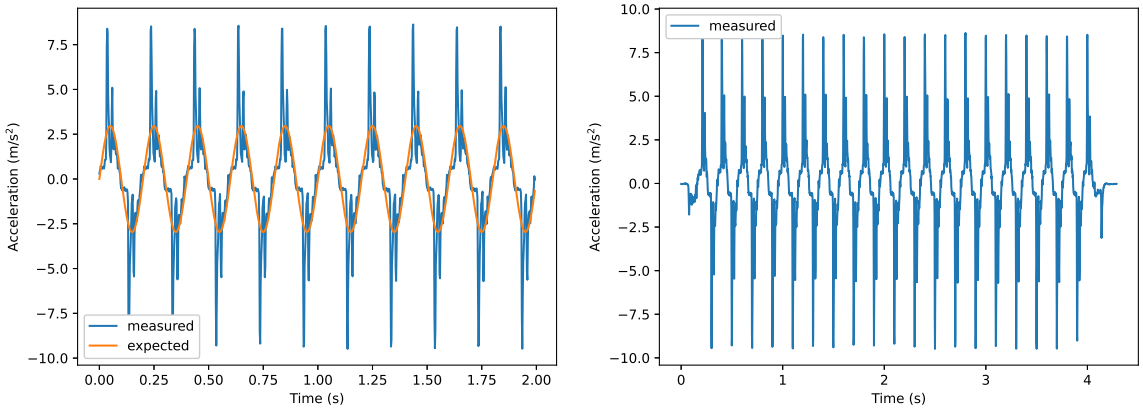

(a) Measured vs. expected comparison. **(b)** Measured acceleration.

Figure D.17: Acceleration data for frequency 5 Hz, crank arm 3 mm, 1 kg payload.

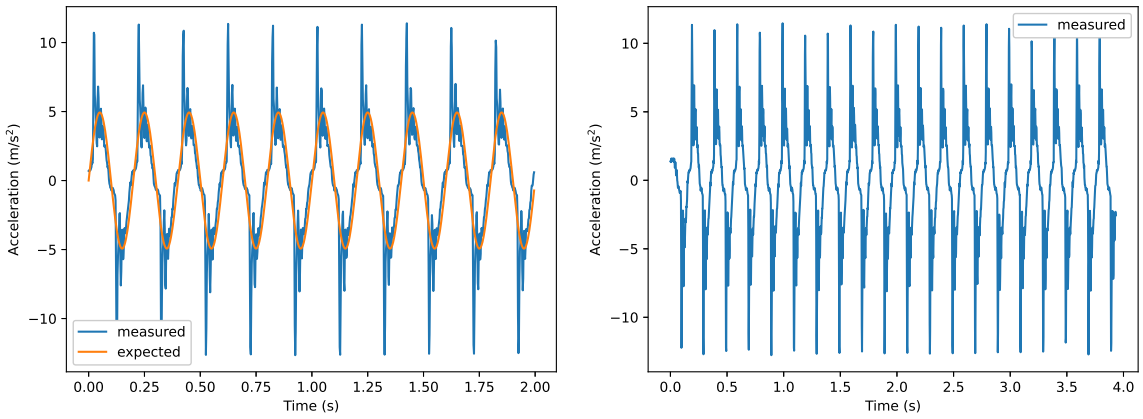

(a) Measured vs. expected comparison. **(b)** Measured acceleration.

Figure D.18: Acceleration data for frequency 5 Hz, crank arm 5 mm, 1 kg payload.

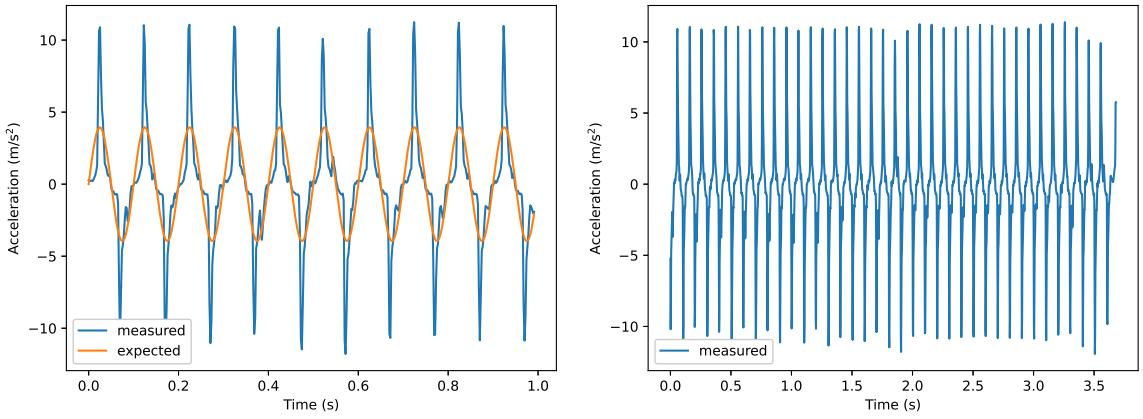

(a) Measured vs. expected comparison. **(b)** Measured acceleration.

Figure D.19: Acceleration data for frequency 10 Hz, crank arm 1 mm, 1 kg payload.

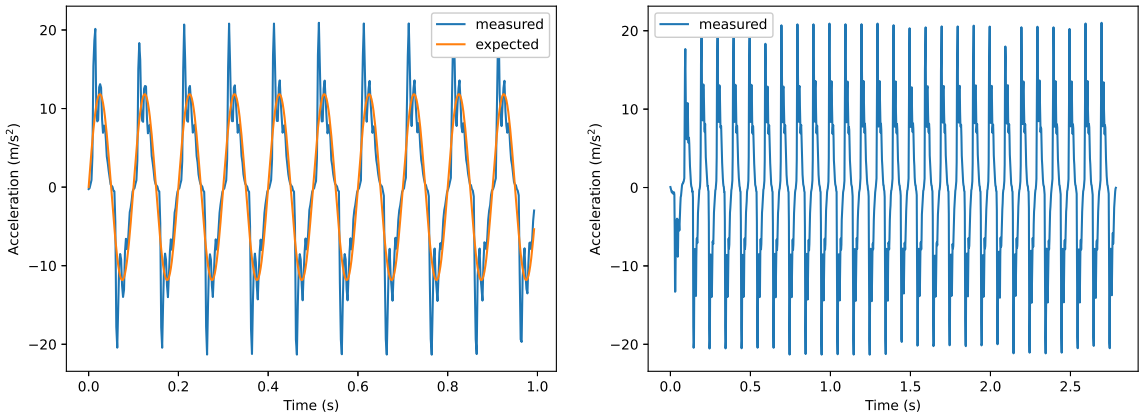

(a) Measured vs. expected comparison. **(b)** Measured acceleration.

Figure D.20: Acceleration data for frequency 10 Hz, crank arm 3 mm, 1 kg payload.

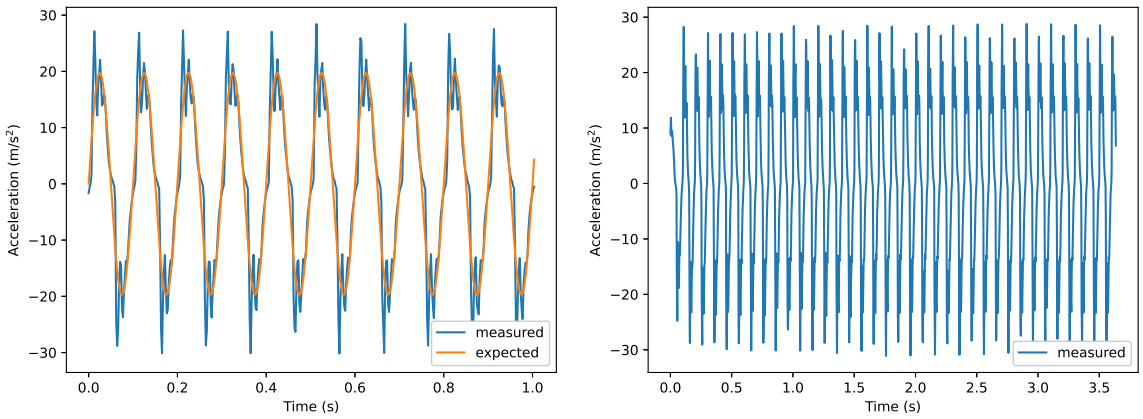

(a) Measured vs. expected comparison. **(b)** Measured acceleration.

Figure D.21: Acceleration data for frequency 10 Hz, crank arm 5 mm, 1 kg payload.

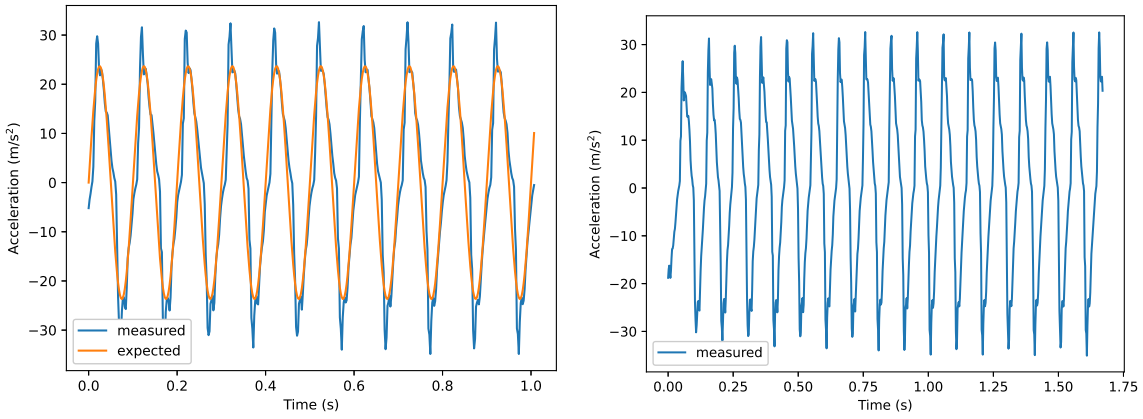

(a) Measured vs. expected comparison. **(b)** Measured acceleration.

Figure D.22: Acceleration data for frequency 10 Hz, crank arm 6 mm, 1 kg payload.

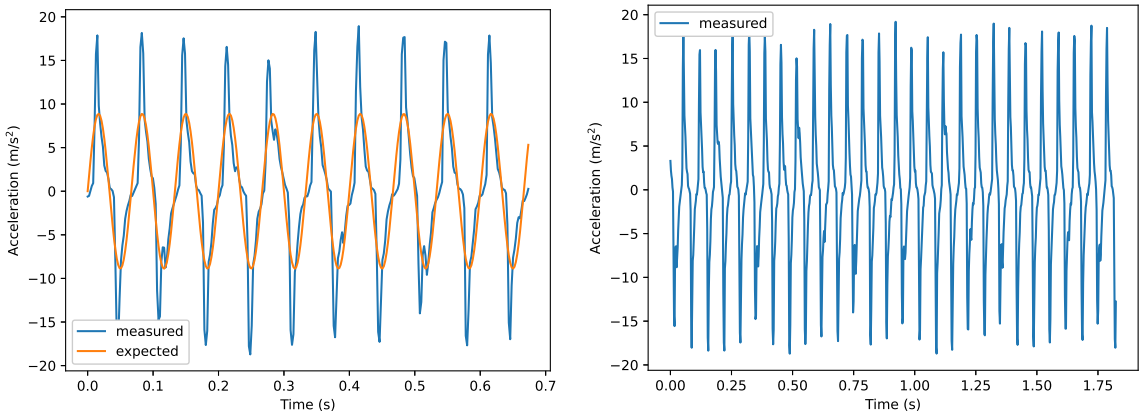

(a) Measured vs. expected comparison. **(b)** Measured acceleration.

Figure D.23: Acceleration data for frequency 15 Hz, crank arm 1 mm, 1 kg payload.

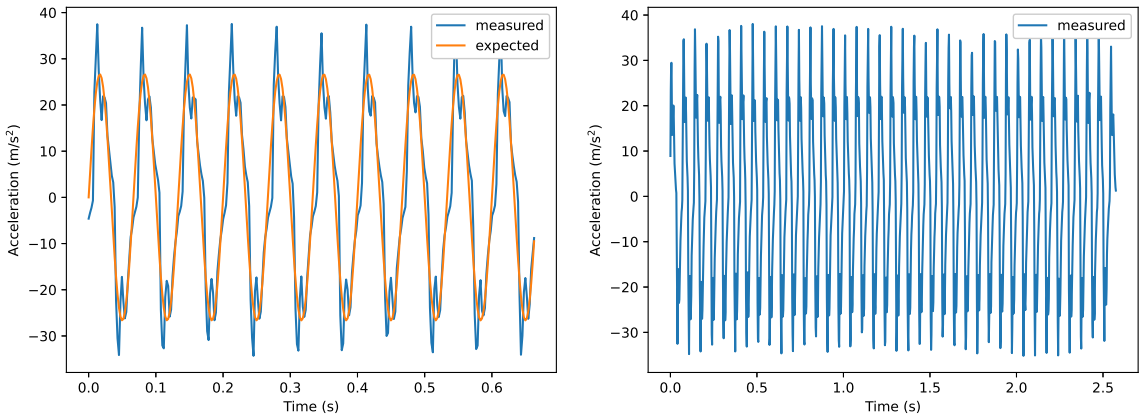

(a) Measured vs. expected comparison. **(b)** Measured acceleration.

Figure D.24: Acceleration data for frequency 15 Hz, crank arm 3 mm, 1 kg payload.

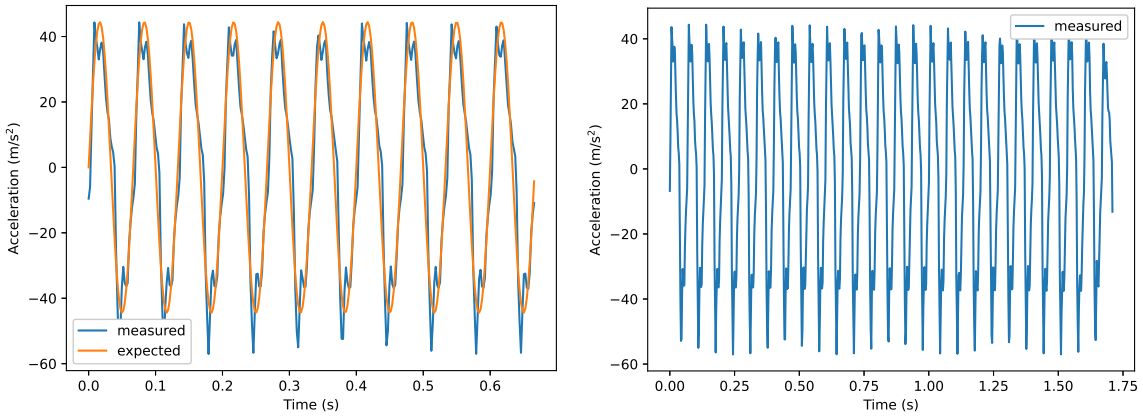

(a) Measured vs. expected comparison. **(b)** Measured acceleration.

Figure D.25: Acceleration data for frequency 15 Hz, crank arm 5 mm, 1 kg payload.

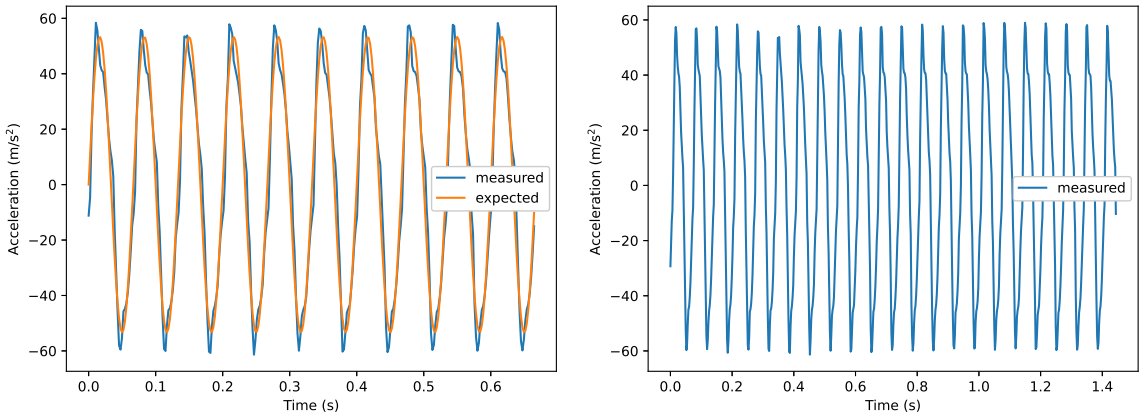

(a) Measured vs. expected comparison. **(b)** Measured acceleration.

Figure D.26: Acceleration data for frequency 15 Hz, crank arm 6 mm, 1 kg payload.

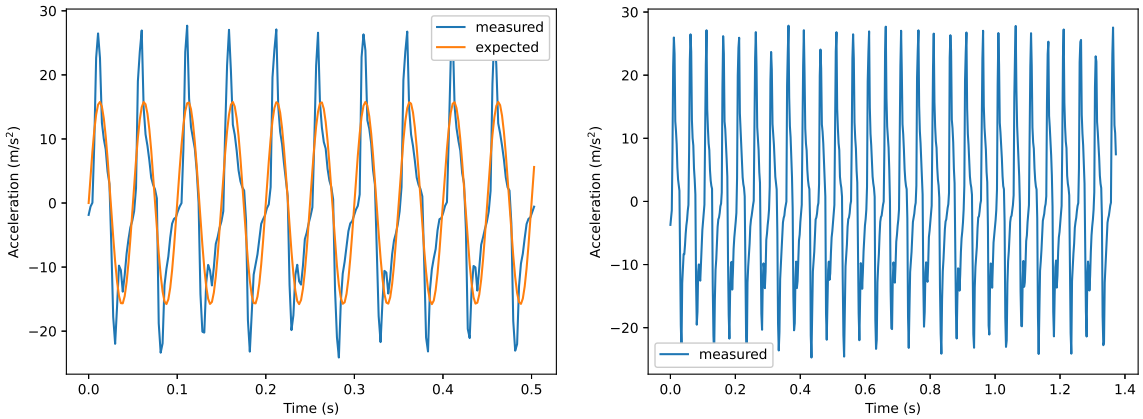

(a) Measured vs. expected comparison. **(b)** Measured acceleration.

Figure D.27: Acceleration data for frequency 20 Hz, crank arm 1 mm, 1 kg payload.

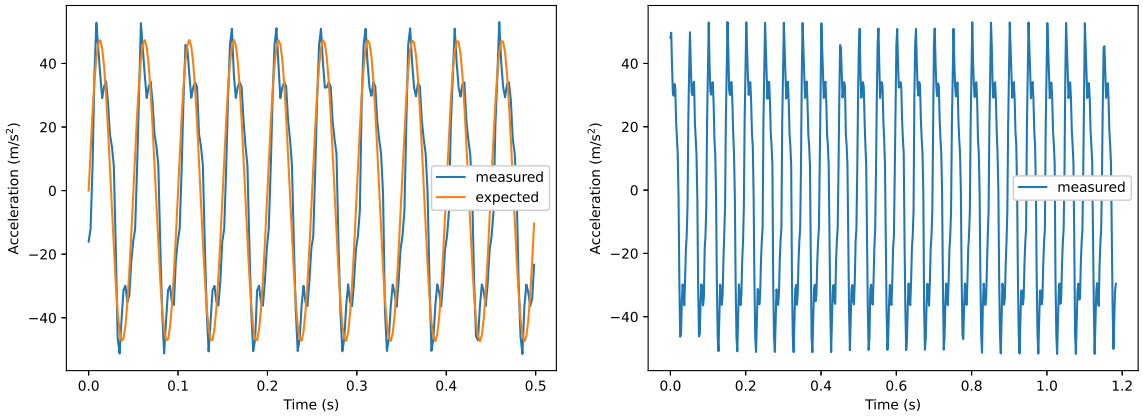

(a) Measured vs. expected comparison. **(b)** Measured acceleration.

Figure D.28: Acceleration data for frequency 20 Hz, crank arm 3 mm, 1 kg payload.

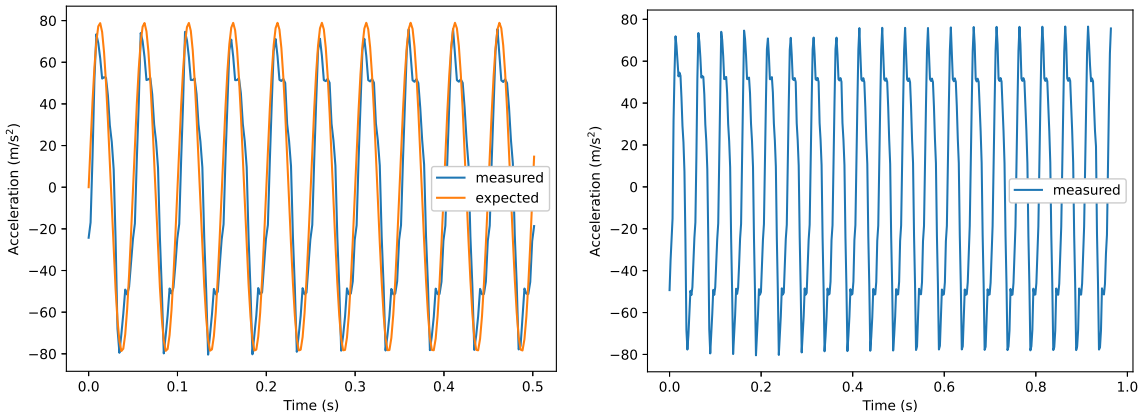

(a) Measured vs. expected comparison. **(b)** Measured acceleration.

Figure D.29: Acceleration data for frequency 20 Hz, crank arm 5 mm, 1 kg payload.

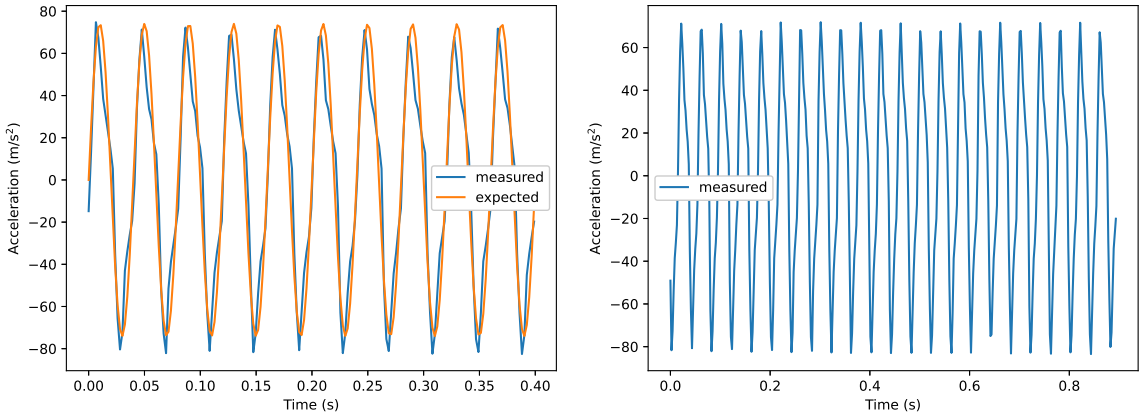

(a) Measured vs. expected comparison. **(b)** Measured acceleration.

Figure D.30: Acceleration data for frequency 25 Hz, crank arm 3 mm, 1 kg payload.

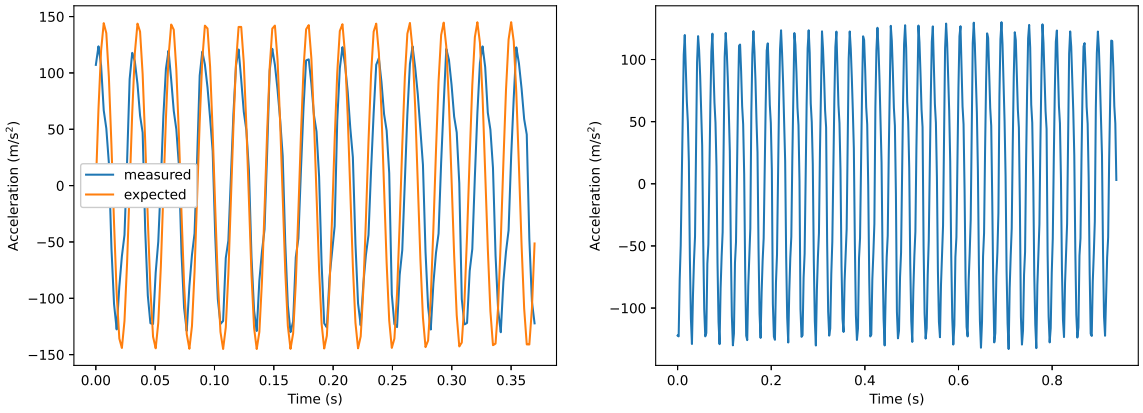

(a) Measured vs. expected comparison. **(b)** Measured acceleration.

Figure D.31: Acceleration data for frequency 35 Hz, crank arm 3 mm, 1 kg payload.

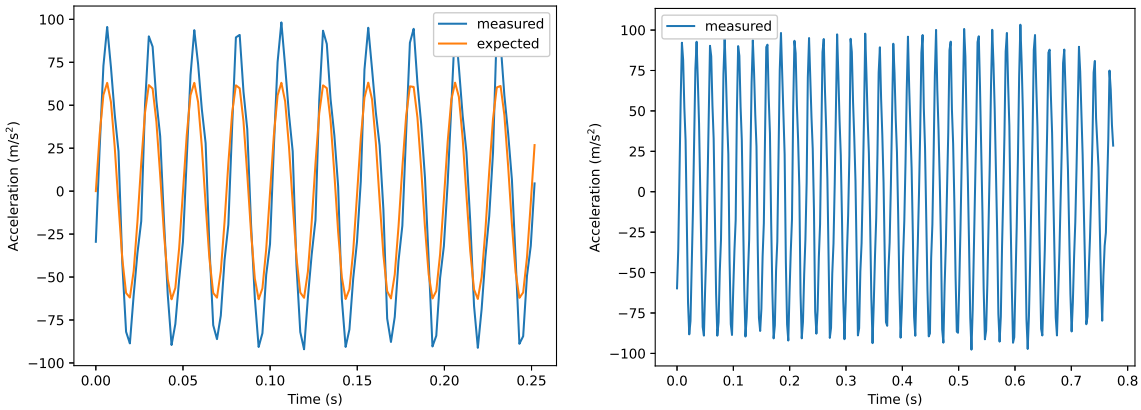

(a) Measured vs. expected comparison. **(b)** Measured acceleration.

Figure D.32: Acceleration data for frequency 40 Hz, crank arm 1 mm, 1 kg payload.